ADVANCED SUSTAINABLE SYSTEMS
www.advsustainsys.com

Why Membranes Matter: Ion Exchange Membranes in Holistic Process Optimization of Electrochemical CO_2 Reduction

*Matthias Heßelmann, Hannah Minten, Tristan Geissler, Robert Gregor Keller, André Bardow, and Matthias Wessling**

Reducing carbon dioxide to value-added chemicals by electrolysis is a promising strategy to substitute fossil-based processes. Research on CO_2 electrolysis has vastly progressed, focusing on catalysis and electrode design, leaving an essential question on the central part of the electrolyzer: Which type of ion exchange membrane is best suited for CO_2 electrolysis from an economic perspective? To address this question, holistic process optimization of CO_2 reduction and product purification is applied. The findings demonstrate that CO_2 electrolysis with an anion exchange membrane shows competitive production costs for CO of 796 €/t_{CO}, outperforming cation exchange and bipolar membranes. Unlike often described, the CO_2 pumping effect does not significantly impair the economics but offers an efficient indirect regeneration of dissociated CO_2. Furthermore, the results emphasize selective reduction of CO_2 rather than co-electrolysis of CO_2 and H_2O. While pointing to a positive economic perspective, life-cycle assessment highlights the need to minimize CO_2 emissions related to electricity consumption and incomplete CO_2 utilization.

1. Introduction

Electrification and defossilization of the chemical industry drive research and development of technologies that utilize renewable electricity and sustainable carbon resources such as CO_2.[1] Future technological developments in this area must focus on substituting fossil-based chemicals with large product volumes and greenhouse gas emissions to reduce the environmental impact of these chemicals significantly.[2,3] Carbon monoxide and its combination with hydrogen as syngas are essential building blocks for the hydrocarbon-based chemical industry, as illustrated in **Figure 1**. The synthesis products from CO and syngas comprise bulk and specialty chemicals, which are either final products or again feedstocks for other processes.[4] Hence, substituting fossil fuel-based reactants with sustainably produced CO or syngas could significantly reduce CO_2 emissions in the chemical industry.

Both CO and syngas can be produced from electrolysis. Instead of fossil fuels such as coal or natural gas, electrolysis utilizes CO_2 and water as reactants and renewable electricity as energy input according to Reactions (1)–(3).

$$CO_2 + H_2O + 2e^- \rightarrow CO + 2OH^- \quad (1)$$

$$2H_2O + 2e^- \rightarrow H_2 + 2OH^- \quad (2)$$

$$2H^+ + 2e^- \rightarrow H_2 \quad (3)$$

Current research on electrochemical CO_2 reduction focuses on decreasing the energy input and improving the CO_2 utilization even when operating at industrially relevant current densities.[5–10] While many of these reports address important aspects to improving CO_2 electrolysis by the development of functional electrode materials, the design of efficient cell configurations, the control of process conditions and reactant transport, one essential question is not yet fully answered: Which ion exchange membrane is the best suited for electrochemical CO_2 reduction in terms of economics?

The ion exchange membrane controls ion transport from one electrolyzer half-cell to the other and affects the reaction

M. Heßelmann, T. Geissler, R. G. Keller, M. Wessling
Chemical Process Engineering
RWTH Aachen University
Forckenbeckstr. 51, 52074 Aachen, Germany
E-mail: manuscripts.cvt@avt.rwth-aachen.de
H. Minten
Chair of Technical Thermodynamics
RWTH Aachen University
Schinkelstr. 8, 52062 Aachen, Germany
A. Bardow
Department of Mechanical and Process Engineering
Energy and Process Systems Engineering
ETH Zürich, Tannenstr. 3, Zürich 8092, Switzerland
M. Wessling
DWI Leibniz-Institute for Interactive Materials
Forckenbeckstr. 50, 52074 Aachen, Germany

The ORCID identification number(s) for the author(s) of this article can be found under https://doi.org/10.1002/adsu.202300077

© 2023 The Authors. Advanced Sustainable Systems published by Wiley-VCH GmbH. This is an open access article under the terms of the Creative Commons Attribution-NonCommercial License, which permits use, distribution and reproduction in any medium, provided the original work is properly cited and is not used for commercial purposes.

DOI: 10.1002/adsu.202300077

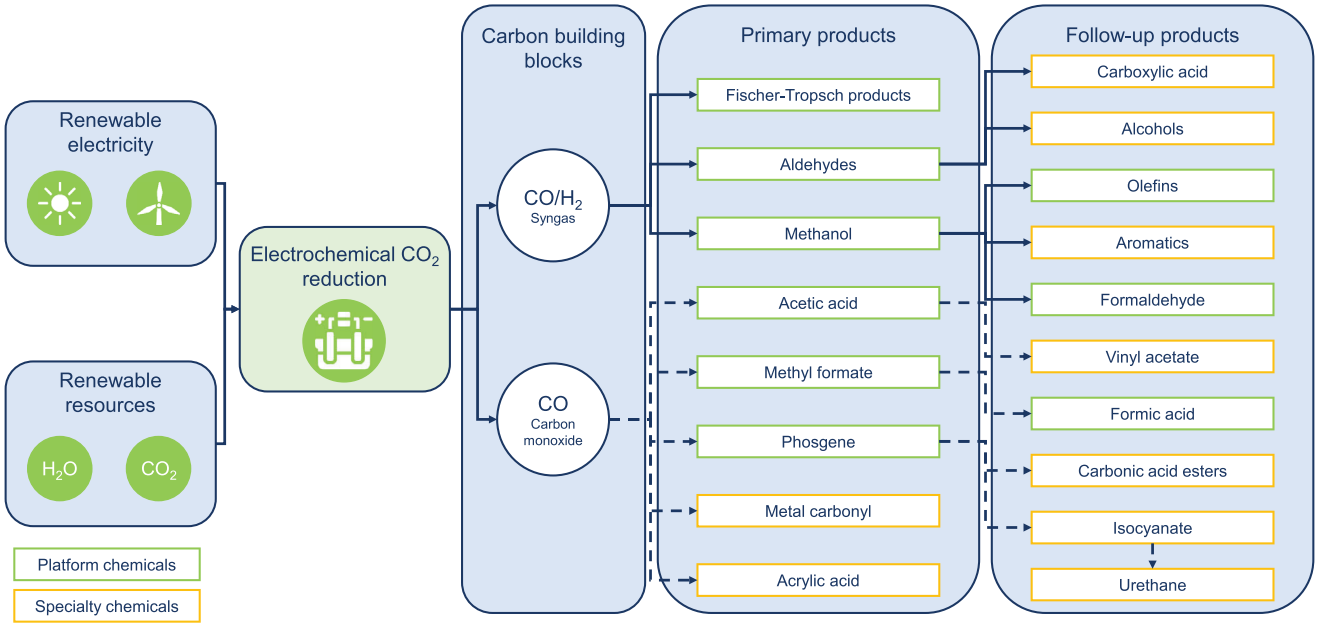

Figure 1. Potential electrochemical products of CO and syngas from renewables and resulting products. Further reactants are not shown for reasons of simplicity.

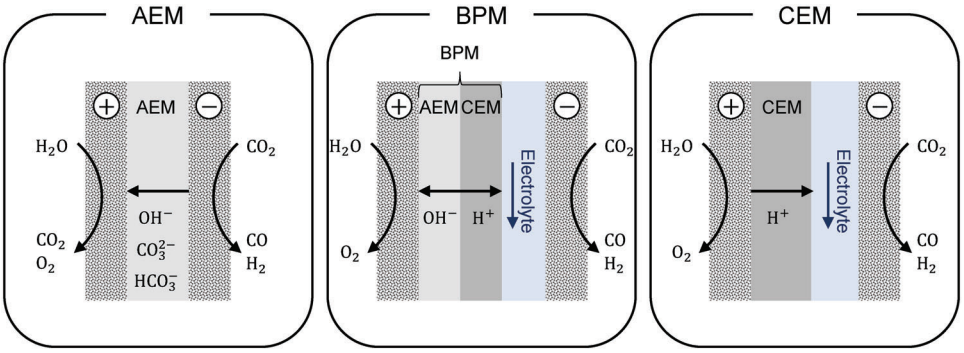

Figure 2. Schematic illustration of the electrolyzer configurations with an anion exchange membrane (AEM) (left), bipolar membrane (BPM) (center), and a cation exchange membrane (CEM) (right). The electrolyzer design configurations are adapted from the experimental works used in this study.[5,11,12]

environment at the electrodes, the mass balance of the whole process, and, thus, the overall electrolyzer performance, that is, Faradaic efficiency, cell voltage, and long-term operation stability. However, the question of which ion exchange membrane is best suited cannot be answered by focusing on the electrolyzer alone because downstream processing will significantly change depending on the membrane type.

Figure 2 presents the three types of ion exchange membranes that are mainly used in CO_2 electrolysis: anion exchange membranes (AEMs) for the selective transport of anions, for example, OH^-, cation exchange membranes (CEMs) for the selective transport of cations, for example, H^+, and bipolar membranes (BPMs), which are composed of an AEM laminated to a CEM. So far, studies on CO_2 electrolysis to CO using AEMs report among the best performance in terms of energy and Faradaic efficiency.[5,13–16] However, a significant drawback often accounted to AEMs is the CO_2 pumping effect due to crossover of HCO_3^- and CO_3^{2-} from the cathodic to the anodic half-cell and the subsequent protonation to CO_2, as illustrated in Figure 2.[17] Ma et al.[16] found that 70% of the gaseous CO_2 at the cathode is captured in the catholyte and transported through the AEM to the anode, where it leaves the process in a mixture with, for example, O_2 from oxygen evolution reaction (OER). Thus, substantial amounts of the reactant are either lost or have to be separated from other gases evolving at the anode, resulting in additional costs. Moreover, AEMs are prone to a combination of chemical and mechanical stability issues, such as polymer degradation in highly basic environment, increased solubility in liquid CO_2 reduction products, and swelling.[18] However, strategies to address these issues can be adapted from other electrochemical applications and comprise crosslinking,[19] reinforcement,[20] and new material design.[21,22]

BPMs can be operated in two modes: the forward bias and the reverse bias mode. In the forward bias mode, the CEM faces the anode, and the AEM faces the cathode. This configuration has the advantage of maintaining a basic pH value in the catholyte, which is beneficial for CO_2 reduction. The CEM prevents the

© 2023 The Authors. Advanced Sustainable Systems published by Wiley-VCH GmbH

crossover of HCO_3^- toward the anode to mitigate CO_2 losses at the anode. On the downside, gaseous CO_2 may be released in the interface between the CEM and AEM, leading to delamination of the membrane.[23] However, several attempts have been developed recently to address the stability issue in the forward bias mode. Kim et al.[24] used a porous ion-conducting sulfonated polymer electrolyte sandwiched by the CEM and AEM to recover evolving CO_2 gas between the membranes. In another approach, Pătru et al.[23] and also O'Brien et al.[25] introduced a bipolar membrane-like configuration by pressing a CEM onto a gas diffusion electrode coated with an alkaline ionomer layer. The thin ionomer layer allows evolving CO_2 to permeate from the interfacial junction back to the electrode without compromising the characteristics of the forward bias mode. Moreover, BPMs with a 3D interfacial junction, as introduced by Shen et al.,[26] can overcome delamination issues due to increased mechanical strength from interpenetrating anion and cation exchange polymer fibers at the CEM–AEM interface.

The reverse bias mode, as shown in Figure 2, has a great advantage compared to using CEM and AEM alone: ion crossover can be mitigated, enabling the use of different electrolytes in the catholyte and anolyte compartments. This degree of freedom is especially advantageous for the electrochemical CO_2 reduction, as it enables using cost-effective, non-noble anode catalysts such as nickel.[27] A direct comparison of the forward and reverse bias modes by Blommaert et al.[28] shows that the reverse bias mode enables more stable product formation by mitigating salt precipitation in the electrode. On the other hand, water dissociation at the membrane junction in the reverse bias mode leads to a significant potential increase. However, using a water dissociation facilitating catalyst layer sandwiched by the CEM and AEM drastically decreases the additional potential increase, as demonstrated in water electrolysis.[29]

The third class of ion exchange membranes used in low-temperature CO_2 electrolysis are CEMs. CEMs such as Nafion are widely used and well established in other electrochemical processes, for example, in fuel cells and water electrolysis and are commercially available on a large scale.[30] The major drawback of using CEMs in CO_2 electrolysis is the typically increased presence of H^+ ions at the membrane surface, which usually requires the implementation of a buffer layer between the membrane and the electrode.[12,13] However, recent studies report notable CO Faradaic efficiencies in acidic zero-gap electrolyzers when using single-atom catalysts such as nickel–nitrogen-doped carbon,[31] employing protective nanocages encapsulating the catalyst,[32] and tuning the ratio of H^+ and alkali cations crossing over from the anolyte.[33]

Several experimental studies discuss the advantages and disadvantages of each membrane type on electrochemical CO_2 reduction.[11,16,17,23,28,34–38] However, future research in the field would benefit from a comparison of the economic and environmental potential of the various electrolyzer configurations.

Techno-economic analyses of CO_2 electrolysis discuss various products and evaluate influencing parameters.[39–46] Only recently, researchers also began to systematically study the techno-economics and environmental impacts of different ion exchange membrane reactors for CO_2 conversion.[44,46] Pribyl-Kranewitter et al.[46] simulated common electrolyzer designs for CO_2 electrolysis to CO and formic acid and product separation in Microsoft Excel and Aspen Plus. However, they only considered fixed operating points without flowsheet optimization. Shin et al.[44] presented an economic evaluation of an AEM and BPM electrolyzer configuration for CO_2 electrolysis. Their results demonstrated that the production costs for CO are competitive with conventional processes. Furthermore, Shin et al. elucidated how the ion exchange membrane can address electrolyte regeneration in CO_2 electrolysis. However, even though the study highlights important aspects regarding the economic assessment and comparison between the AEM and BPM electrolyzer configuration, the simplified representation of the processes does not allow a profound evaluation of mass and energy balances and, thus, investment and operational costs. Therefore, the literature needs a holistic approach to identifying an optimal process configuration and operation point of electrolysis and downstream processing to minimize the overall production costs of electrochemical CO_2 reduction products. Roh et al.[47] presented a globally optimized process for flexible operation of electrochemical CO_2 reduction and separation of the product stream. Yet, they only considered a one-side buffered CEM electrolyzer configuration which might be less efficient and profitable compared to other electrolyzer configurations. Furthermore, Roh et al. did not model the downstream processing on a detailed level. However, the separation process needs rigorous consideration to investigate the achievable purities of the desired products and assess recycle streams and losses in the overall process.

In this work, we present a holistic approach to optimize and assess the economics of the electrochemical CO_2 conversion to CO or syngas by accounting for different electrochemical membrane reactor configurations. The mass and energy balances for each electrolyzer are based on state-of-the-art literature data. The downstream processing of the anodic and cathodic gas outlet streams is implemented using membrane gas permeation. Membranes offer unique advantages in terms of flexible operation, scalability, and costs, making them a viable option for downstream processing of the electrolysis off-gases.[48–50] The process flowsheet and operational parameters are optimized to minimize the specific production costs of the desired product.

Additionally, the cost-optimal system configuration is examined regarding its environmental impacts in a life-cycle assessment (LCA) and benchmarked with state-of-the-art processes to assess the potential of substituting conventional synthesis routes. A few publications have been dedicated to the LCA and carbon footprinting of low-temperature electrochemical CO_2 reduction.[46,51,52] However, they either do not consider CO or syngas as products or use simplified assumptions for process data. Therefore, we investigate the environmental impact of electrochemical CO_2 reduction and its benchmark technologies to identify mitigation potentials. We derive process optimization strategies for minimizing the global warming impact (GWI) and investigate potential burden-shifting to other areas of environmental damage.

With our work, we can therefore elucidate the following research questions on electrochemical membrane reactors and holistic process design:

- Which electrolyzer configuration is most economical for CO and syngas production?
- Which process parameters are key to increasing profit?

© 2023 The Authors. Advanced Sustainable Systems published by Wiley-VCH GmbH

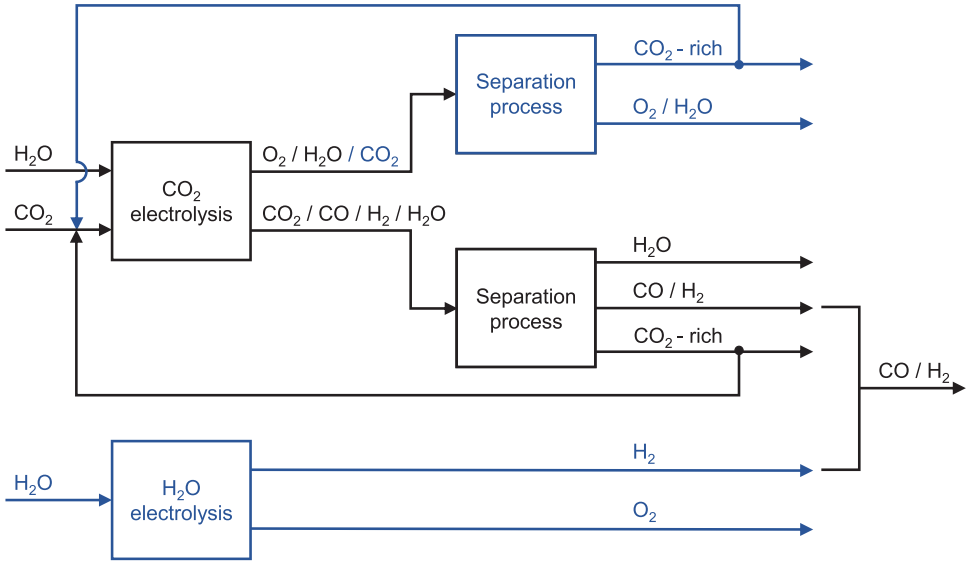

Figure 3. Simplified block flow diagram of the process for electrochemical CO and H_2 production from CO_2 and H_2O. The blue blocks and streams are only considered for the AEM electrolyzer and the production of H_2 in water electrolysis, respectively.

- Is it economical to operate CO_2 electrolysis to produce both carbon monoxide and hydrogen as syngas?
- Does the CO_2 pumping effect in AEMs negatively influence the overall process economics as often described, or could it offer advantages?
- How does the optimized CO_2 electrolysis process compete with alternative processes economically and environmentally?
- How can the GWI of CO_2 electrolysis further be decreased?

2. Results and Discussion

Holistic process optimization has been employed to determine the optimal process flowsheet and operating conditions of electrochemical CO_2 reduction to CO or syngas.

Figure 3 sketches the process layout: CO_2 and H_2O are converted to CO and H_2 in an electrolyzer. Experimental data from state-of-the-art CO_2 electrolysis literature is used to fit regression models that account for energetics and mass conversion.[5,11,12] Here, the most prominent electrolyzer configurations in low-temperature CO_2 electrolysis using AEMs, BPMs, and CEMs are compared. The cathodic product stream is purified in the separation process to meet the desired specifications. In this work, the downstream processing of the gaseous products is achieved by adsorptive drying and membrane gas permeation. For the AEM electrolyzer configuration, CO_2 crossover is considered, and the amount of CO_2 in the anodic off-gas being purified and recycled or emitted to the atmosphere is an optimization task. For syngas production, additional H_2 is purchased from H_2O electrolysis. The ratio of H_2 produced in CO_2 electrolysis and H_2 purchased is a degree of freedom in the optimization. The desired products in this study are CO with a purity of ⩾98% as, for example, used in phosgene production, and syngas with H_2:CO ratios of 1:1 and 2:1 used, for example, in oxo-synthesis and Fischer–Tropsch synthesis, respectively.[53–55] For scaling the syngas processes, the product streams are set to the same heating value as the CO product gas stream. A more detailed description of the model and the process units is given in the Experimental Section.

The objective of the holistic optimization is to minimize the specific production costs (€/$t_{product}$) of the overall process by adapting the process configuration, that is, the process flowsheet, the ratio of recycle and purge streams, and the selection of the gas permeation membrane materials, as well as relevant process parameters, that is, the current density of the electrolyzer, the electrode area, the compression ratio, and the gas permeation membrane area. Based on the process optimization, economics, and environmental impacts are investigated.

The environmental impact of electrochemical CO_2 reduction to CO and syngas are investigated by evaluating the economically optimized process setup using the LCA methodology.[56,57] Our LCA study identifies the main contributors to the environmental impact of electrochemical CO_2 reduction using a holistic set of impact categories.[58] Applying different decarbonization scenarios, electrochemical CO_2 reduction is benchmarked to current synthesis routes of CO or syngas. By assessing electrochemical CO_2 reduction and competing processes in comparison, this study aims to provide a frame of reference for the environmental impact and its drivers. Moreover, potential areas for process improvement in terms of GWI are derived.

2.1. Electrochemical Membrane Reactor Configuration for CO and Syngas Production

The specific production costs for CO using the AEM electrolyzer, as shown in **Figure 4**, are 796 €/t_{CO} and lower than those using the BPM and CEM reactor with 837 €/t_{CO} and 1 071 €/t_{CO}, respectively. The CO prices from conventional state-of-the-art production processes reported in the literature cover a wide range from 522 €/t_{CO} to 1 070 €/t_{CO} attributed to uncertainties in the source of CO.[39,42] Thus, the CO_2 electrolysis processes considered in this study already achieve competitive CO production costs.

© 2023 The Authors. Advanced Sustainable Systems published by Wiley-VCH GmbH

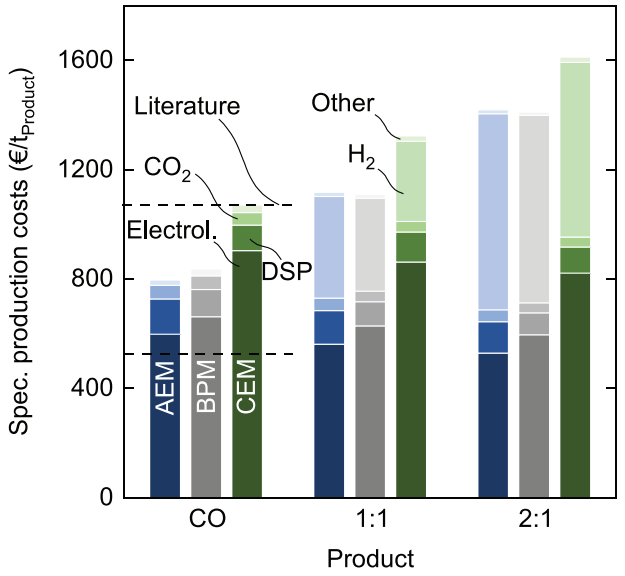

Figure 4. Specific production costs for the different reactor configurations and products CO and syngas (1:1, 2:1), respectively. The costs are divided into expenditure for the electrolysis process (Electrol.), the downstream processing (DSP), the reactants CO_2 and H_2, as well as other process-related expenditures like CO_2 emission costs and costs for deionized water. The electrolysis and the downstream processing expenses comprise investment, operational, replacement, and maintenance costs. The dashed lines represent CO prices from the literature.[39,42]

The electrolyzer is the main cost driver in CO production and constitutes 75–84% of the total production costs. Similar values are reported in the literature.[44] The costs for electrolysis are mainly responsible for the cost difference between the three electrolyzer configurations and are the lowest for the AEM electrolyzer.

The expenditures for separating the product gases are slightly higher for the AEM reactor, making up 16% of the total production costs. The higher downstream processing costs are attributed to the additional separation of the anodic off-gas due to the crossover of CO_2, which is about 8% of the total production costs. A similar share of anodic downstream processing costs of ≈6%, that is, 18 €/t_{CO} assuming linear depreciation and the currency conversion factor used in our study, was also reported by Shin et al.[44] It needs to be mentioned that the plant capacity in the work of Shin et al. is about a factor 4.6 smaller compared to this study. Therefore, lower operational and capital expenditures lead to deviations in absolute costs.

The optimized flowsheet presented in **Figure 5** assumes a CO_2:O_2 ratio of 2:1 in the anodic gas outlet stream of the AEM electrolyzer, which means that the crossover of CO_3^{2-} dominates. In the base case scenario, the optimization results that it is more economical to recycle CO_2 with a purity of ⩾ 98% than emitting it.

The flowsheets for the BPM and CEM electrolysis processes for CO production are presented in Figures S5 and S6, Supporting Information. At the operation point of the BPM and CEM electrolyzers, listed in **Table 1**, the Faradaic efficiency of CO is about 89% and 82%, respectively. Thus, substantial amounts of H_2 are co-produced but not purified and are not considered an additional valuable product when pure CO is the target product. In future work, implementing a second objective function—the minimization of H_2 production costs—could improve the economics of the BPM and CEM electrolysis processes and make them more competitive. In the optimized flowsheets, the permeate stream of the second membrane step is mainly recycled into the gaseous feed of the electrolyzer. The mole fraction of CO_2 in the feed thereby decreases to about 70 mol%, for example, for producing pure CO using a BPM electrolyzer. In this work, it is assumed that the decreased CO_2 feed fraction does not have an impact on the electrochemical CO_2 reduction, which is valid for CO_2 fractions between 60 mol% and 100 mol% as shown by Kim et al.[59] At higher potentials, as considered in the work of Kim et al., a further decrease in the CO_2 feed fraction, however, would lower the production rate of CO due to mass transport limitations.[60] In future work, more rigorous models of the electrolysis process need to be implemented in the optimization model to consider the detrimental effect of decreasing CO_2 feed fractions at high current densities.

For the production of syngas with ratios of 1:1 and 2:1, the process using the BPM electrolyzer shows the lowest specific production costs with 1 111 €/t_{syngas} and 1 411 €/t_{syngas}, respectively. The respective flowsheets of the two processes are given in **Figures 6** and **7**. Low downstream processing expenditures and costs for additional H_2 result in lower production costs compared to the AEM and CEM electrolyzer when using the BPM electrolyzer. However, the AEM electrolysis process costs are in a similar range. For both syngas products, the costs for electrolysis with the CEM configuration strongly dominate due to a high cell voltage and large electrode areas needed, even though more H_2 is produced in the CEM electrolyzer than in the other two. The specific production costs and the flowsheets of the BPM electrolysis processes show that most of the H_2, that is, ≈87% contained in the syngas is purchased from water electrolysis. The amount of purchased H_2 is even higher for the 2:1 ratio (93%). The same applies to the other electrolyzer configurations as shown in Figures S7–S10, Supporting Information. In turn, the CO_2 electrolyzer is operated at a point where mostly CO is produced in syngas production. These findings emphasize that CO_2 electrolysis should be used and optimized for CO production only and not for the co-production of CO and H_2. For syngas production, a combination with water electrolysis is economically more promising.

The electrolyzer constitutes 39–69% of the overall capital expenditures (CAPEX) for the AEM and CEM electrolyzer in CO production, as shown in the left graph in **Figure 8**. The wide range is mainly attributed to the different operating current densities of 230 and 58 mA cm^{-2} as identified in the holistic optimization as a trade-off between CAPEX and operational expenditures (OPEX). The lower current density leads to a significantly larger electrolyzer area for the CEM configuration to achieve the required production rate. Assuming the CEM electrolyzer in the base case scenario can operate at industrially relevant current densities (200 mA cm^{-2}),[61] the CAPEX can be reduced by 50% due to the smaller electrode area. But more impactful is the decrease in the related catalyst and CEM replacement costs by 30%, resulting in specific production costs of ≈ 870 €/t_{CO}. Thus, considering the aforementioned recent progress in acidic CO_2 electrolysis, it might become more profitable in the future.

Compared to CO production, the decrease in the expenses for the production of syngas is attributed to the lower production

© 2023 The Authors. Advanced Sustainable Systems published by Wiley-VCH GmbH

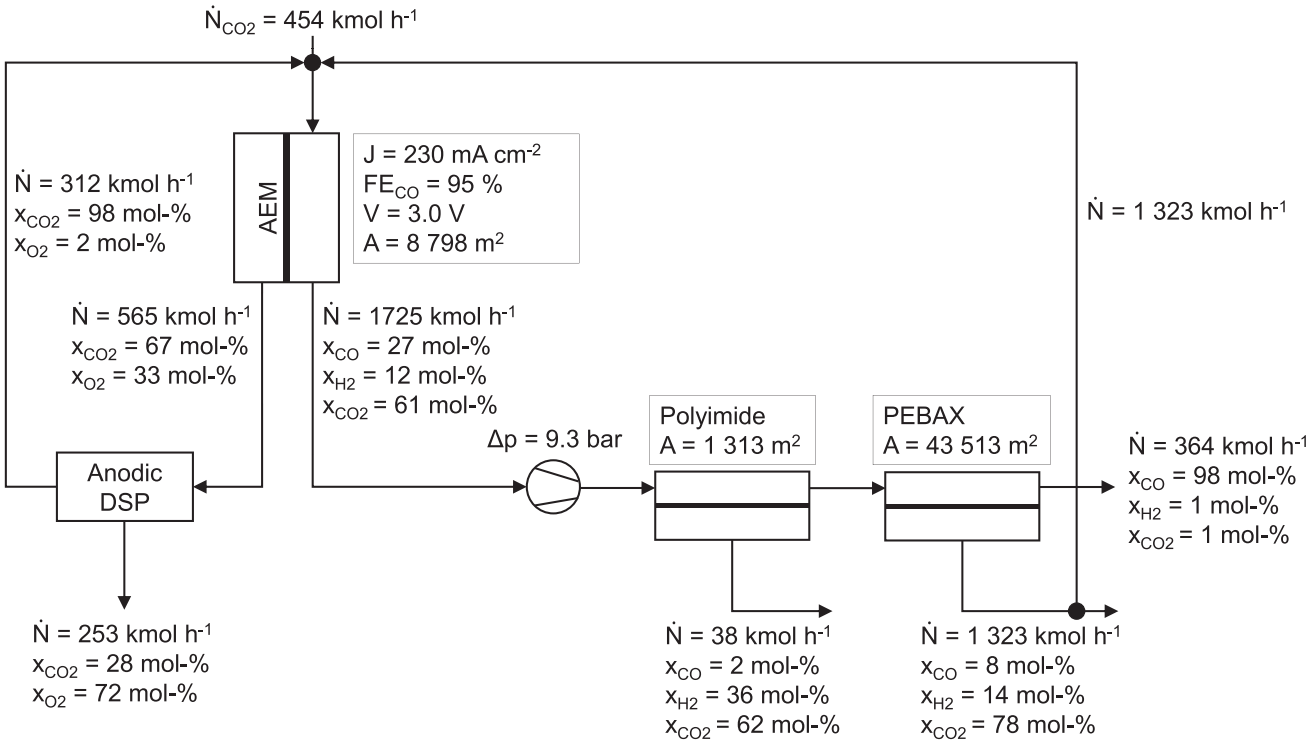

Figure 5. Flowsheet of electrochemical CO production using an AEM electrolyzer for the base case scenario. The water removal unit is not shown in the flowsheet, as only the costs for water removal are taken into account. The anodic downstream processing is only shown as a block because it is not modeled rigorously in the overall process flowsheet but is considered as a surrogate model. The gas permeation membrane materials used in the process are Polyimide and PEBAX, a trademark from Arkema.

Table 1. Key operational parameters of the electrolyzer in the base case scenario.

Parameter	AEM	BPM	CEM	Unit
Current density	230	70	58	mA cm^{-2}
Cell voltage	3.0	2.8	3.0	V
CO Faradaic efficiency	95	89	82	%
Per-pass conversion	20	20	20	%
Anodic CO_2:O_2 ratio	2:1	–	–	–

capacity and purity of CO from CO_2 electrolysis and the lower effort for downstream processing as the total product flow rate decreases when keeping the heating value of the product stream constant. The distribution of investment costs between the electrolysis and downstream processing are fairly similar for the different products.

The right graph in Figure 8 shows that the OPEX for electrolysis dominates. The OPEX of the AEM and BPM processes are fairly similar. The main cost driver of electrolysis is the electricity demand. The electricity costs account for 92% and 75% of the electrolysis-related OPEX for the AEM and CEM electrolyzer, respectively. The share of electricity costs is lower for the CEM electrolyzer even though the electricity demand is greater (60 MW for AEM and 70.4 MW for CEM). The increased electricity demand is attributed to the worse energetics of the CEM compared to the AEM electrolyzer. The underlying experimental data for the AEM (Liu et al.[5]) electrolyzer was generated in a zero-gap cell assembly, whereas a one-sided buffered cell design was chosen for the CEM electrolyzer (Vennekötter et al.[12]). As the acidic environment of the CEM promotes hydrogen evolution reaction (HER) at the cathode, the buffer layer is typically necessary between the cathode and the membrane, causing additional ohmic voltage losses.[12,13] However, some studies demonstrate that CO_2 reduction may work in an acidic or zero-gap assembly with a CEM showing superior CO_2 utilization rates compared to AEM electrolyzers.[32,33,62–65] Yet, most of these studies are not on the level of buffered CEM and AEM characteristics in terms of Faradaic efficiency and cell voltage. Only most recently, Li et al.[31] achieved up to 95% CO Faradaic efficiency and 3.6 V at a current density of 500 mA cm^{-2} using a Ni–N–C catalyst in a CEM zero-gap electrolyzer design. Even though the work of Li et al. shows a promising perspective for acidic CO_2 electrolysis, long-term stability of the process and the Ni–N–C catalyst was only shown for a few hours with a decrease in Faradaic efficiency, a loss of electrode hydrophobicity, and slight formation of carbonate salt visible after only 8 h of the experiment. The remaining electrolysis-related OPEX are attributed to replacement costs, which have an increased influence on the economics of the CEM electrolysis process. IrOx needs to be used as an anode catalyst in the AEM and CEM configuration because of the neutral to acidic pH in the anolyte.[66] The use of the noble catalyst material results in increased electrolyzer replacement costs which are even more pronounced for the CEM electrolyzer due to the large electrode areas which need to be replaced. Thus, these costs show a more

© 2023 The Authors. Advanced Sustainable Systems published by Wiley-VCH GmbH

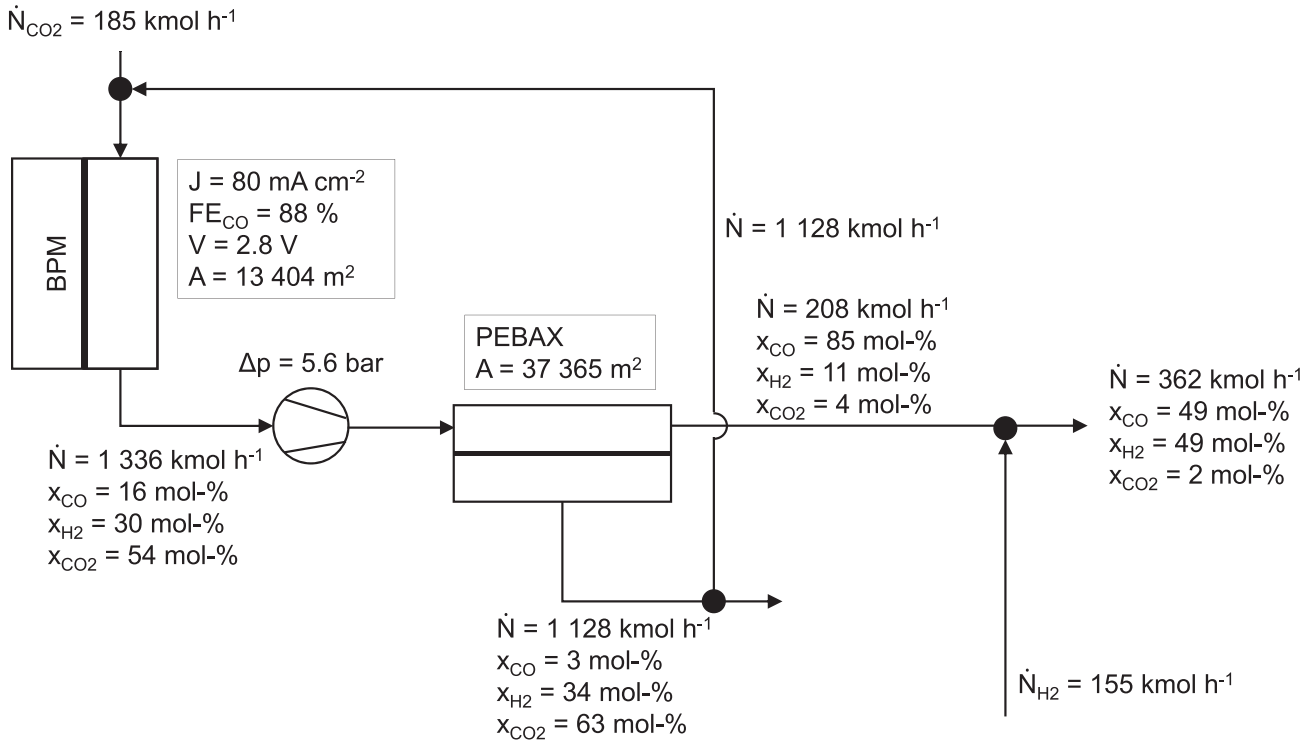

Figure 6. Flowsheet of electrochemical syngas (ratio 1:1) production using a BPM electrolyzer for the base case scenario. The water removal unit is not considered in the flowsheet, as only the costs for water removal are taken into account. The gas permeation membrane material used in the process is PEBAX.

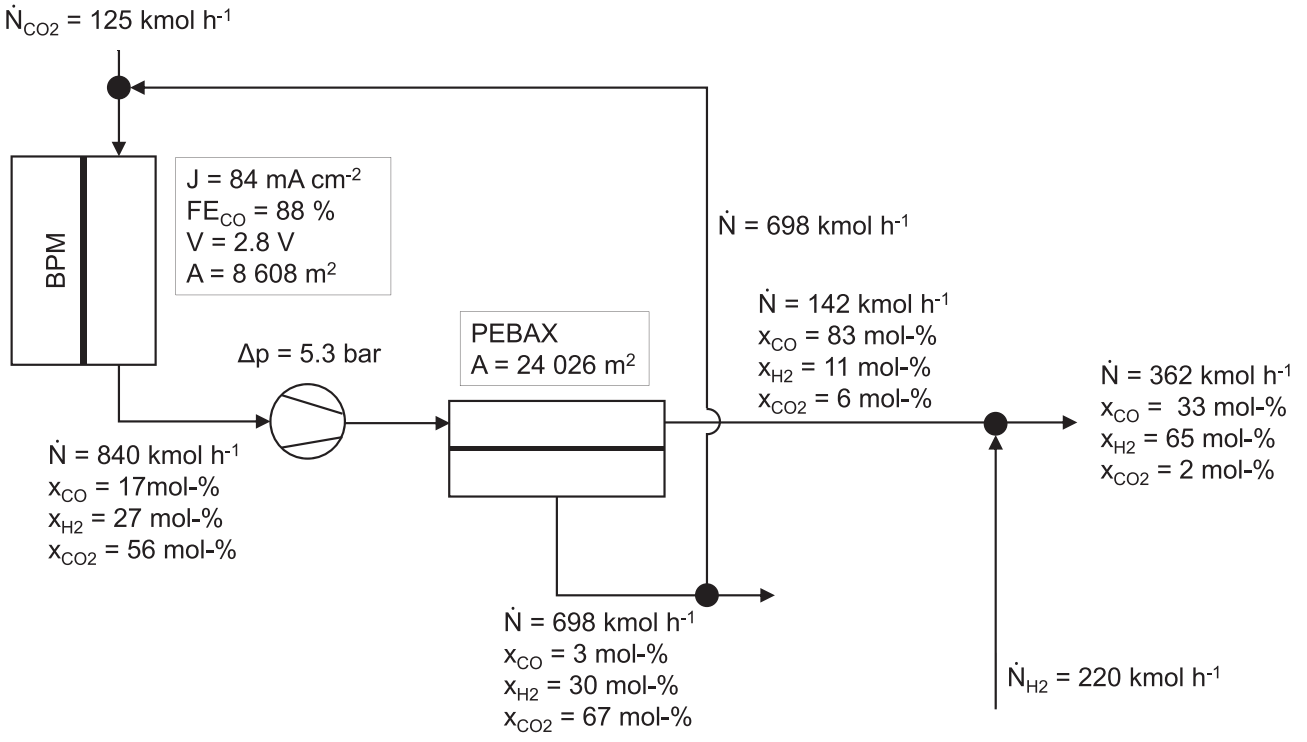

Figure 7. Flowsheet of electrochemical syngas (ratio 2:1) production using a BPM electrolyzer for the base case scenario. The water removal unit is not considered in the flowsheet, as only the costs for water removal are taken into account. The gas permeation membrane material used in the process is PEBAX.

© 2023 The Authors. Advanced Sustainable Systems published by Wiley-VCH GmbH

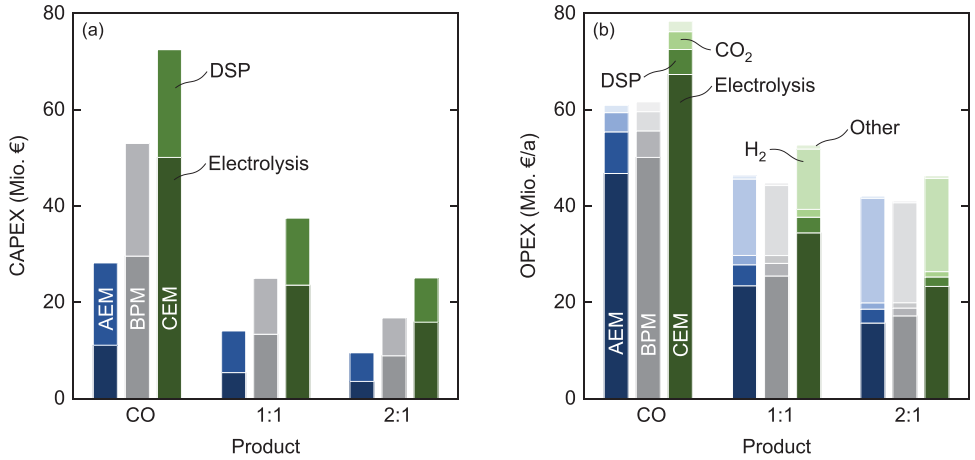

Figure 8. a) CAPEX and b) OPEX for the different reactor configurations and production of CO and syngas (1:1, 2:1), respectively. The heating value is kept constant for the three products. The CAPEX comprises investment costs for CO_2 electrolysis and costs for downstream processing. In this study, H_2 from water electrolysis is purchased and only considered in the OPEX. The OPEX comprises expenses related to the electrolysis, the downstream processing, the reactants CO_2 and H_2, and other operation-related expenditures. The electrolysis and downstream processing OPEX include electricity costs and components replacement. Minor expenditures, that is, costs for deionized water and maintenance, are summed up to other process-related costs. A more detailed overview of the different cost contributors is specified in the Experimental Section.

Table 2. Economic and technical parameters considered in the sensitivity study.

Parameter	Worst case	Base case	Best case	Unit
Electricity price	0.135	0.09	0.045	€/kWh
Bare module costs electrolyzer	+30	0	−30	%
CO_2 feedstock price	45	22	0	€/t_{CO_2}
CO_2 certificate price	50	25	0	€/t
Cell voltage	+40	0	−40	%
Faradaic efficiency CO	−20	0	+20	%
Per-pass conversion	10	20	30	%

significant contribution (8%) to the electrolysis-related OPEX compared to the BPM electrolysis process (1.6%).

2.2. Sensitivity of Economics Toward Uncertainties

The previous results highlight that electrochemical CO_2 reduction should be applied and optimized for the selective electrochemical reduction of CO_2 to CO and not for the co-electrolysis to syngas. Therefore, the following results and discussion focus on the production of pure CO only. Attributed to the low maturity level of CO_2 electrolysis and the associated uncertainty of technical end economic parameters, the sensitivity of the production costs toward changes in the most relevant influencing factors is assessed. The process flowsheet and operation point are optimized for each scenario in **Table 2**. The operating parameters of the electrolyzers in the best and worst case scenarios are given in Tables S4–S6, Supporting Information.

The most significant influence on the specific production costs in **Figure 9** is seen for a change in electricity price: The electricity price of the basic scenario is assumed to be 0.09 €/kWH according to the German industry electricity price from 2017.[67] The variation of the price by +50% covers the expected German industry electricity price of 2030, assuming the phase-out of coal-fired power generation.[68] The lower limit of −50% is, for example, reached by Norway, whose electricity production is solely based on hydropower.[69] The change in electricity costs affects both the CO_2 electrolysis and the downstream processing. However, due to the minor contribution of the downstream processing costs to the overall production costs, as presented in Figure 4, the significant sensitivity toward the electricity price is mainly attributed to the electrolysis process. The electricity costs for the AEM, BPM, and CEM electrolysis processes account for 67.5%, 63.8%, and 59.1% of the specific production costs. The impact of the electricity price on the AEM electrolysis process is slightly more pronounced compared to the BPM and CEM process configurations due to the higher share of electricity costs for the AEM electrolyzer, as mentioned before. However, despite the significant contribution of electricity costs to the production costs of the AEM electrolysis process, the absolute production costs are still comparatively low due to the superior energetics of the electrolyzer.

The bare module costs of the electrolyzers have been calculated based on material costs for the main components, that is, the electrode catalysts, the ion exchange membrane, the housing, and the periphery. In the basic scenario, the costs are calculated to 1 050 €/m^2 for the AEM, 780 €/m^2 for the BPM, and 1 030 €/m^2 for the CEM electrolyzer configuration. These costs are in a comparable range to those reported in the literature.[39,40,42] When varying the bare module costs between −30% and +30%, the specific production costs respond nearly linear to the change as shown in Figure 9. A symmetric deflection in the tornado charts expresses a linear response of the specific production costs as it can also be taken from the line diagrams in Figures S12–S17, Supporting Information. The CEM electrolyzer process configuration shows the highest sensitivity toward electrolyzer investment costs. Intuitively, an increase in electrolysis capital costs would be compensated by decreasing the electrode area. That, in

© 2023 The Authors. Advanced Sustainable Systems published by Wiley-VCH GmbH

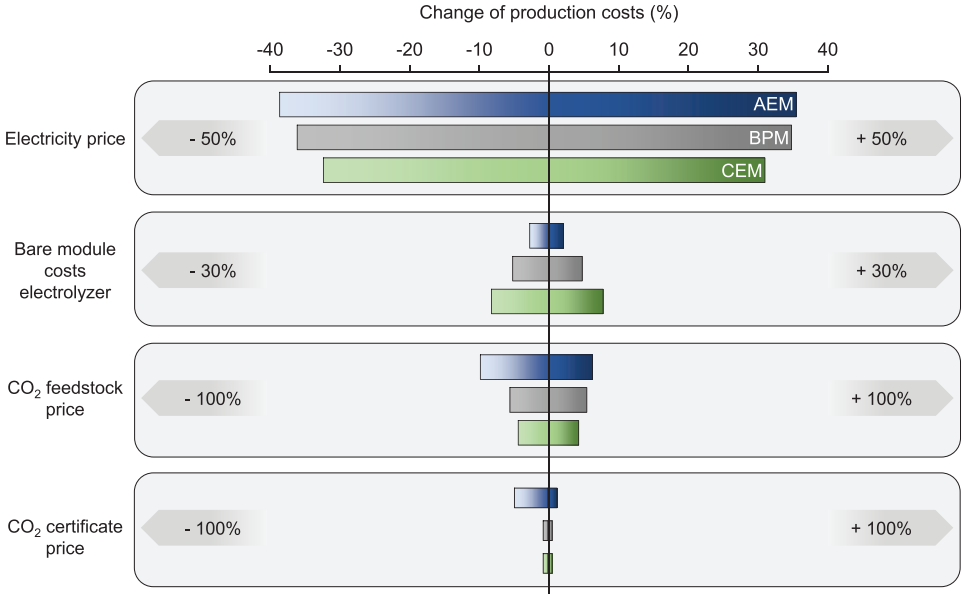

Figure 9. Sensitivity of the different reactor configurations for CO production toward a change in economic parameters.

turn, increases the current density of the electrolyzer to maintain the desired production capacity of the plant. Such a relationship can be seen for the AEM electrolyzer in Figure S18, Supporting Information, where the change in the bare module costs is compensated by the change in electricity costs due to the variation of the current density. Consequently, the specific production costs show negligible sensitivity to the capital costs of the electrolyzer. However, due to the poor energetics of the CEM electrolyzer, the electrode area, and the current density are only varied slightly by the optimizer for a change in bare module costs. Therefore, the CAPEX for the electrolysis is only partially balanced, leading to higher and lower production costs when increasing and decreasing the bare module costs, respectively.

The sensitivity of specific production costs toward the CO_2 price and the CO_2 emission costs behave similarly. Production costs using the BPM and CEM electrolyzer exhibit a nearly linear change. The impact of the CO_2 price is more pronounced than the one of CO_2 emission costs because of the larger contribution to the overall production costs, as shown in Figure 4. The optimizer does not vary the operation point of the electrolyzer for the different scenarios in both sensitivity parameters. However, an increase in the CO_2 price or the CO_2 emission costs increases the overall CO_2 utilization rate, meaning less loss of CO_2 in the downstream processing. The CO_2 utilization rate is the share of CO_2 in the feed gas that is converted to the final product CO. Between the worst case scenario and the best case scenario of the CO_2 price, the CO_2 utilization rate varies between 90%–85% for the BPM and 87%–81% for the CEM electrolyzer (same values for the CO_2 emission costs). The change in utilization rate is mainly attributed to the amount of CO_2 that is lead out in the permeate stream of the first gas permeation membrane step. When increasing the CO_2 price or the CO_2 emission costs, the membrane is scaled down by the optimizer, and so is the CO_2 flux through the membrane. The non-linear trend in the AEM electrolysis process toward the CO_2 price and the CO_2 emission costs is attributed to a change in the process flowsheet: At a certain point for decreasing CO_2 prices (19 €/t_{CO_2}) and CO_2 emission costs (20 €/t_{CO_2}), the anodic off-gas is not separated anymore but emitted to the environment. The change in treating the off-gas leads to a more pronounced decrease in the CO production costs because additional costs for the anodic downstream processing are omitted.

The electrolysis process contributes most to the overall process cost and reacts most sensitively to changes in economic parameters. Hence, further optimization of the electrolyzers is required. **Figure 10** therefore shows how the change of relevant technical electrolysis parameters influences process economics. In the sensitivity study of the cell voltage, the output data of the regression models, that is, the polarization plots, are shifted by +/− 40% from the base case scenario plots. The cell voltage significantly influences the CO production costs. Furthermore, cell voltage variations solely affect the operation of the electrolyzer but not the downstream processing when keeping the product requirements constant. Therefore, the sensitivity trend in the tornado chart toward the cell voltage is fairly linear. Moreover, due to the high share of electricity costs for electrolysis in the production costs with the AEM electrolyzer process, the change in cell voltage shows a more pronounced influence. The operation point of the AEM electrolyzer changes from 230 mA cm^{-2} (3 V) to 405 mA cm^{-2} (1.9 V) and 158 mA cm^{-2} (4 V) in the best and worst case scenarios, respectively. Thereby, the electricity demand increases from the best to the worst case scenario from 38 to 80 MW, and the electrode size increases from 5000 to 12 800 m^2.

The CEM electrolyzer process shows the lowest sensitivity toward a change in Faradaic efficiency for CO. Even though in the best case scenario, the CEM electrolyzer allows to operate at a point with Faradaic efficiencies for CO of up to 89% at current

© 2023 The Authors. Advanced Sustainable Systems published by Wiley-VCH GmbH

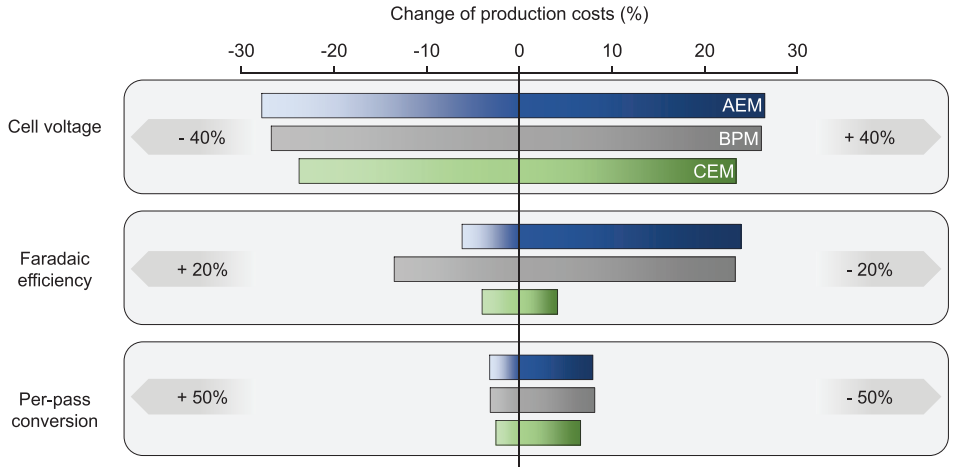

Figure 10. Sensitivity of the different reactor configurations for CO production towards a change in technical parameters of the electrolyzer.

densities below 40 mA cm^{-2}, the operation point of the electrolyzer is not varied significantly from the basic scenario (58 mA cm^{-2} and 82% Faradaic efficiency for CO). In the worst and best case scenarios, the current density of the electrolyzer is optimized to 55 mA cm^{-2} (79% Faradaic efficiency for CO) and 61 mA- cm^{-2} (85% Faradaic efficiency for CO), respectively. Thus, mostly energetics but also capital costs of the electrolyzer determine the operation point even when the Faradaic efficiency is improved. However, recent trends in acidic zero-gap CO_2 electrolysis can overcome the poor energetics and mass transport issues at elevated current densities in buffered CEM configurations by reducing ohmic voltage losses and suppressing detrimental carbonate formation.[31]

In contrast, the AEM and BPM electrolysis processes are more susceptible to variations in the Faradaic efficiency. It must be noted that for the AEM and BPM electrolyzer, an increase of the Faradaic efficiency by ≈5% and ≈12% already lead to an efficiency of 100%, resulting in a nonlinear trend in the tornado charts. For the BPM electrolyzer, the operation point is optimized to 70 mA cm^{-2} (71% Faradaic efficiency for CO) and 111 mA cm^{-2} (100% Faradaic efficiency for CO) in the worst and best case scenario, respectively. In the worst case scenario, the current density is not changed significantly compared to the base case scenario (68 mA cm^{-2} and 89% Faradaic efficiency for CO) as higher current densities would lead to even lower Faradaic efficiencies and also higher cell voltages. However, larger electrode areas are needed at the lower current density to achieve the required production capacity. Hence, the energy demand of the electrolyzer increases from 60 MW in the base case to 75 MW in the worst case. The expenses for the downstream processing also increase between the base and worst scenarios by 44%. At large, the increase in electrolysis and separation costs leads to the strong influence of Faradaic efficiency on production costs. Consequently, improvements in mass transport of CO_2 to the catalyst sites and suppression of the HER in BPM electrolyzers, by, for example, modification of the gas diffusion electrode using functional ionomers, could improve the process economics.[8,70] Most AEM electrolyzers reported in the literature already reach high Faradaic efficiencies for CO production because of the alkaline environment at the cathode and the resulting absence of H^+ ions.[5,7,22,71] The strong sensitivity when decreasing the Faradaic efficiency, however, underlines the importance of investigating and optimizing long-term stability in AEM electrolyzers to maintain a constant operating point. Xu et al.,[71] for example, presented a self-cleaning strategy by periodic operation of the electrolyzer and were able to operate at constant Faradaic efficiency for more than 157 h. Furthermore, Petrov et al.[72] showed that casting membranes with internal micro channels significantly improves water management and potassium crossover, increasing energy efficiency and long-term stability of CO_2 electrolyzers.

The per-pass conversion of CO_2 to CO is 20% in the base case scenario and is varied between 30% (+50%) and 10% (−50%). The variation of the per-pass conversion causes a non-linear change in specific production costs with a more pronounced sensitivity to a decrease in the per-pass conversion than an increase. The lower per-pass conversion leads to a dilution of the cathodic gas stream and, when keeping the desired production capacity constant, also to a larger gas flow rate in the downstream processing. The electrolyzer is not scaled, and the optimizer does not change the operating point when varying the per-pass conversion. Thus, the elevated specific production costs are mainly attributed to increased energy consumption in the compression and larger gas permeation membrane areas to separate CO_2. For the AEM electrolyzer, for example, the share of costs for downstream processing in the overall production costs increases from 16% to 22% when changing the CO_2 per-pass conversion from 20% to 10%. Additionally, the CO_2 utilization rate decreases for the lowest per-pass conversion, for example, from 85% to 73% for the CEM electrolyzer. Thus, larger expenditures for CO_2 emissions and replenishment need to be considered for lower CO_2 per-pass conversions.

Interestingly, an increase in the per-pass conversion to state-of-the-art values of around 20–30% reported by different groups[9,73,74] does not significantly improve the specific

© 2023 The Authors. Advanced Sustainable Systems published by Wiley-VCH GmbH

production costs. When increasing the per-pass conversion, less unconverted CO_2 is in the downstream flow of the electrolyzer, thus lowering the CO_2 mole fraction and the total flow rate of the cathodic gas outlet stream. The lower flow rate reduces the downstream processing unit sizes, whereas the lower partial pressure of CO_2 in the downstream needs to be compensated by an increase in compression ratio to maintain a sufficient driving force for gas permeation. As the compressor is the main cost driver in the downstream processing, the trade-off between unit size and compression ratio mainly causes the non-linear behavior in Figure 10 when changing the per-pass conversion. To overcome this trend, alternative technologies for gas purification could be considered, for example, absorption and adsorption.

The sensitivity toward the per-pass conversion is similar for all three electrolyzer configurations but with a slightly lower amplitude for the CEM electrolyzer due to a lower share of downstream processing costs in the production costs. It must be mentioned that a change in per-pass conversion is assumed not to affect the electrolysis process. However, in real systems, the per-pass conversion results from many influencing factors, for example, the CO_2 feed flow rate and composition, the electrolyte, the structure and composition of the gas diffusion electrode, and the temperature and pressure. Thus, changes in these parameters would also affect the operation of the electrolyzer and, therefore, expenditures for electrolysis. Furthermore, Jeng et al.[74] showed that increasing the per-pass conversion by decreasing the CO_2 feed flow rate also increases the fraction of CO_2 being converted to carbonates. Thus, also increased costs for the anodic downstream processing are expected.

In summary, the sensitivity study highlights three major influencing factors on the economics of the CO_2-to-CO electrolysis process: the electricity price, the cell voltage, and the Faradaic efficiency. Therefore, the future development in CO_2 electrolysis process needs to focus on decreasing the electricity demand of the electrolyzer as well as improving the reactant mass transport. The AEM electrolyzer configuration already shows promising results due to the energetically efficient zero-gap cell design and the favorable conditions at the electrode. However, a major obstacle often associated with the application of AEMs in CO_2 electrolysis is the HCO_3^- and CO_3^{2-} crossover, which leads to the evolution of CO_2 at the anode side.[17,28] Therefore, the following section deals with this subject in more detail.

2.3. CO_2 Crossover in AEM Reactors

Figure 11 presents the specific production costs for CO and the CO_2 utilization rate of the overall process for different CO_2:O_2 ratios which refer to the crossover of solely OH^- (0:1), CO_3^{2-} (2:1), or HCO_3^- (4:1). The specific production costs are the lowest for a CO_2:O_2 ratio of 0:1, at which no CO_2 evolves at the anode and no purification of the anodic off-gas or expenditure for CO_2 emission costs is required. The costs increase by ≈8.5% when CO_3^{2-} becomes the dominant permeating species indicating that the expenditures for the anodic downstream processing do not contribute significantly to the overall process costs, as mentioned before. When the CO_2:O_2 ratio changes from 2:1 to 4:1 for HCO_3^- crossover, the specific production costs do not increase significantly. In the anodic downstream processing, CO_2 is

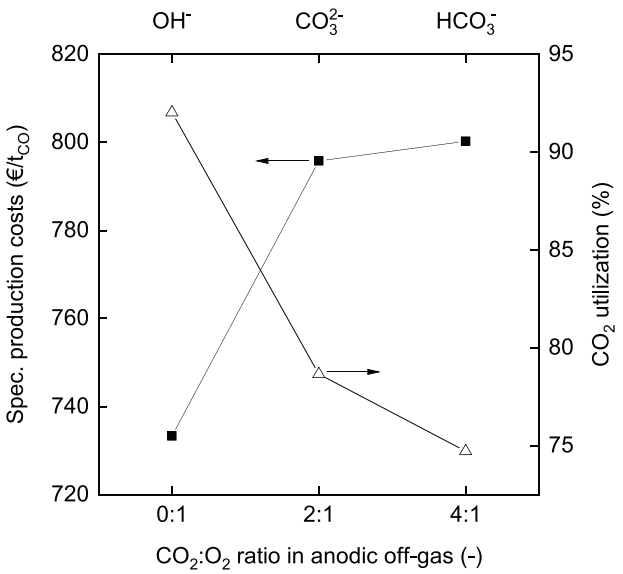

Figure 11. Specific production costs and CO_2 utilization rate for an AEM electrolyzer and the production of CO at different CO_2:O_2 ratios in the anodic off-gas. The different CO_2:O_2 ratios result from the crossover of either OH^-, CO_3^{2-}, or HCO_3^-.

concentrated in the permeate of the two-step membrane gas permeation process. As gas permeation is a partial pressure-driven process, increasing the concentration of the faster-permeating component in the feed results in a higher driving force for separation. Hence, the expenditures for purification of the anodic off-gas only increase slightly because of the higher flow rate of CO_2 evolving at the anode. Simultaneously, the CO_2 utilization of the overall process decreases from 92% to 79% and 75% when CO_3^{2-} and HCO_3^- become the dominant permeating species in the AEM. The lower CO_2 utilization for the case of CO_2 evolution at the anode is attributed to the higher loss of CO_2 in the anodic downstream processing.

Summarizing, CO_2 pumping does not significantly impair the economics of the AEM-based process even for the highest CO_2:O_2 ratio, when membrane gas permeation is used to separate CO_2 and O_2. Moreover, the recovery of gaseous CO_2 from CO_3^{2-} and HCO_3^- crossed over the AEM implies an additional advantage over the BPM and CEM electrolyzers.

Rabinowitz et al.[17] discuss the problem of CO_2 loss via carbonate formation in low-temperature CO_2 electrolysis. The energy needed to regenerate CO_2 from CO_3^{2-} in the liquid electrolyte is ideally 56 kJ $mol_{CO_2}^{-1}$ ($|\Delta G^0|$), but realistically >230 kJ $mol_{CO_2}^{-1}$.[17,75] For the BPM and CEM electrolyzer, where CO_3^{2-} is transported out of the electrolyzer in the catholyte outlet, the additional energy penalty for regeneration of CO_2 from CO_3^{2-} needs to be considered.

In the AEM electrolyzer, CO_3^{2-} is assumed to be the dominant ion transferring across the ion exchange membrane in the considered current density range and for long operation times.[7,16] CO_3^{2-} is protonated to CO_2 at the anode and leaves the electrolyzer. As more than 80% of the CO_2 evolving at the anode is recycled to the cathode, CO_3^{2-} is thereby indirectly regenerated. However, an additional energy penalty needs to be considered

© 2023 The Authors. Advanced Sustainable Systems published by Wiley-VCH GmbH

Table 3. Comparison of the specific energy demand for separating the anodic off-gas compared to literature and the ideally required Gibbs free energy of mixing.

	Ideal	Our work	Alerte et al.[45]	Shin et al.[44]
Separation technology	-	Gas permeation	Amine absorption	Pressure swing adsorption
CO_2:O_2 ratio	2:1	2:1	2:1	1:1
Energy demand (kJ $mol^{-1}_{CO_2}$)	2.3	22.2	2 501	1.3
Comment	Calculation in Supporting Information	Base case	Without heat integration	Based on shortcut calculation method

for the protonation of CO_3^{2-} at the anode side due to the shift in pH and, thus, an increase in the OER overpotential.[76] In this study, the increased overpotential is already included in the experimental data, which is used to fit the regression model of the electrolyzer.

The energy required to separate CO_2 from O_2 in the anodic off-gas using membrane gas permeation is calculated to be 22 kJ $mol^{-1}_{CO_2}$. **Table 3** compares the specific energy demand for the separation of CO_2 and O_2 to the literature. The thermodynamically required energy for separating the gas mixture is 2.3 kJ $mol^{-1}_{CO_2}$. Alerte et al.[45] report a value of 2 501 kJ $mol^{-1}_{CO_2}$ for the anode gas separation using amine absorption. The enormous energy demand results from the high heating duty in the amine regeneration. Therefore, amine scrubbing might not be a suitable technology for the anodic off-gas separation because: 1) it is usually not applied for CO_2 fractions >25% and 2) certain amines tend to degrade when brought in contact with O_2.[77,78] Shin et al.[44] employed pressure swing adsorption for the separation of a 1:1 mixture of CO_2 and O_2. Their shortcut calculation results in an energy demand of 1.3 kJ $mol^{-1}_{CO_2}$ which is less than the absolute standard Gibbs free mixing energy of 3.4 kJ $mol^{-1}_{CO_2}$ for the 1:1 mixture, calculated from Aspen Plus V11. The contradiction highlights the importance of more rigorous consideration of the separation process.

In summary, the indirect regeneration of CO_2 from the electrolyte by the ionic crossover of carbonate and subsequent separation of the anodic off-gas using membrane gas permeation is energetically more favorable than regenerating CO_2 directly from the electrolyte by for example, a calcination cycle.[75] Thereby, the CO_2 pumping effect is a cost saver than a cost killer, as often described. Moreover, even higher energy efficiency and better economics could be achieved when using a liquid-to-liquid anode reaction without oxygen evolution, as demonstrated by Xie et al.[79]

2.4. Life-Cycle Assessment of Optimized Process

The most economical process configuration is selected for an environmental assessment. The studied configuration produces pure CO with an AEM electrolyzer and a two-step membrane separation process on the cathode side, as shown in Figure 5. **Table 4** provides all in- and outputs of the electrochemical CO_2 reduction process.

Conventionally, pure CO is produced from steam methane reforming (SMR) with subsequent CO separation. Additionally, we consider water electrolysis with subsequent reverse water-gas-shift (rWGS) as an alternative CO_2-based route for CO production.[80] Since SMR co-produces H_2 and CO in a 3:1 molar ratio, the process is multi-functional. The LCA standards define two appropriate solutions for multi-functionality to ensure a fair comparison of process alternatives: substitution and system expansion. We apply system expansion in our study to avoid potentially misleading negative impacts.[81] Consequently, the functional unit is defined as the production of 1 kg CO and 0.216 kg H_2, which corresponds to a 3:1 (H_2:CO) molar ratio. H_2 required to fulfill the functional unit for CO_2-based CO production is supplied from alkaline water electrolysis, as discussed in the Experimental Section. The primary motivation for developing carbon capture and utilization processes is decreasing the GWI of chemical production. Thus, the following section focuses on the GWI, while results in other impact categories are presented in Figure S19, Supporting Information. Since cradle-to-gate system boundaries are applied in our assessment, some carbon is incorporated and temporarily fixed in the product leaving the system boundary. Hence, negative GWI results are possible in cradle-to-gate studies with CO_2 capture. Typically, the incorporated carbon is released to the air as CO_2 emissions at the end-of-life (e.g., combustion) of the product. In this study, the amount of carbon incorporated into the product leaving the system boundaries corresponds to 1.57 kg CO_2-eq of combustion CO_2 emissions per functional unit. **Figure 12** shows the total GWI with incorporated ("fixed") CO_2 separately to avoid potentially misleading negative GWI values.

Table 4. In- and outputs of the studied process configuration.

Inputs	Amount	Unit
Water	4.01	kg
CO_2 feedstock	1.96	kg
Electricity (AEM electrolyzer)	5.86	kWh
Electricity (anodic downstream processing)	0.30	kWh
Electricity (cathodic downstream processing)	0.39	kWh
Outputs	**Amount**	**Unit**
CO	1	kg
Heat (byproduct)	0.02	kWh
H_2O (emitted)	3.99	kg
CO_2 (emitted)	0.41	kg
O_2 (emitted)	0.59	kg

The environmental impact of carbon capture and utilization processes is heavily influenced by external parameters such as the CO_2 source and the environmental impacts of electricity and heat.[81] Thus, we calculate LCA results using four scenarios for

© 2023 The Authors. Advanced Sustainable Systems published by Wiley-VCH GmbH

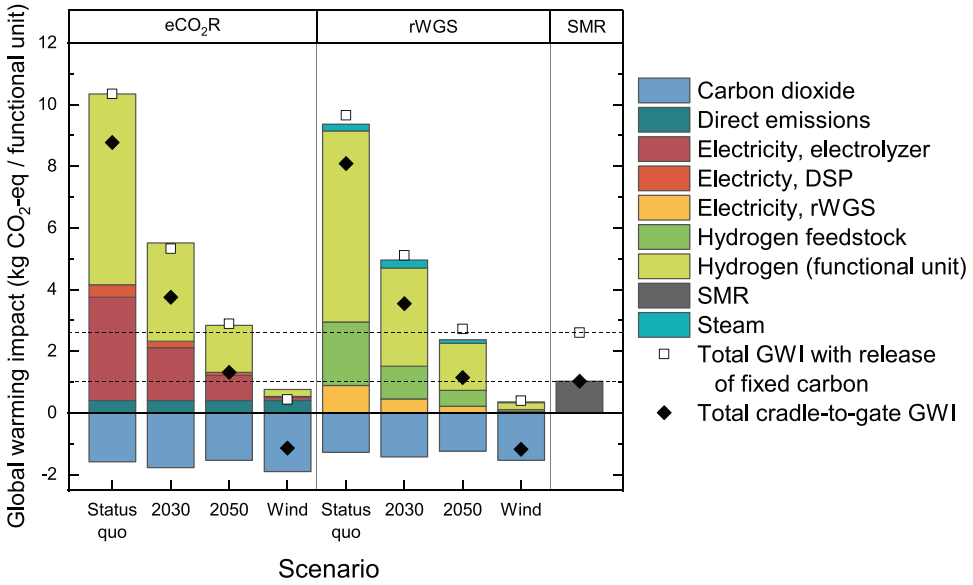

Figure 12. Global warming impact (GWI) of electrochemical CO_2 reduction to CO using an AEM electrolyzer compared to reference technologies for CO production. For a fair comparison of the processes, the functional unit is expanded to 1 kg CO and 0.216 kg H_2. The scenarios represent increasing levels of decarbonization for CO_2, electricity, and heat supply. The dashed lines refer to the total GWI with the release of fixed carbon and the total cradle-to-gate GWI of the benchmark process steam methane reforming (SMR).

Table 5. Overview of scenarios used in this LCA study.

	Status quo	EWI 2030	EWI 2050	Wind electricity only
Electricity	German mix 2018	EWI 2030	EWI 2050	Wind electricity
Heat	Natural gas boiler	From electricity	From electricity	From electricity
CO_2 source	Coal-fired power plant	Coal-fired power plant	Direct air capture	Direct air capture

feedstock CO_2, electricity, and heat. The scenarios represent decarbonization levels of the process inputs, as listed in **Table 5**.

For the production of 1 kg of CO and 0.216 kg H_2, the cradle-to-gate GWI of electrochemical CO_2 reduction is 8.77 kg CO_2-eq in the status quo scenario. The GWI is dominated by electricity production emissions, mainly for AEM electrolyzer operation and H_2 production. With a decreasing GWI of electricity, the CO/H_2 production GWI decreases up to a (cradle-to-gate) minimum of −1.36 kg CO_2-eq when only wind electricity is employed. In the wind electricity scenario, direct emissions of the AEM electrolyzer process contribute over 50% of carbon emissions, replacing electricity as the dominating contributor to GWI.

The conventional fossil-based SMR route has a cradle-to-gate GWI of 1.04 kg CO_2-eq., which is lower for electrochemical CO_2 reduction only in the wind power scenario. The advantage of the SMR process is the co-production of H_2, which is replaced by energy-intensive water electrolysis in the CCU systems. Therefore, the CCU systems can mitigate emissions only with an electricity mix based majorly on renewable energy sources or if H_2 production becomes less emission-intensive, for instance, through efficiency improvements.

Comparing electrochemical CO_2 reduction to an alternative CO_2-based route puts the contribution analysis results into context and allows insights into process competitiveness. Thus, GWI contributors are investigated for water electrolysis with subsequent rWGS. For the rWGS route, H_2 production is the largest contributor to the GWI. However, since H_2 instead of water is used as feedstock for the process, the reactor electricity demand is lower than for electrochemical CO_2 reduction. Furthermore, the rWGS route causes fewer direct CO_2 emissions due to higher rates of CO_2 utilization of ≈100%[80] compared to 79% for the electrochemical route. Consequently, less CO_2 must be captured for the process. In total, rWGS achieves a slightly lower GWI than electrochemical CO_2 reduction, with the difference in GWI decreasing with increasing decarbonization levels.

Although rWGS performs slightly better in terms of GWI, the total GWI is nearly equal for both routes, especially at high decarbonization levels. Naturally, this study uses data from the laboratory, which usually differs from upscaled process data.[82] These data gaps are inherent for both compared CO_2-based routes, which is why the environmental superiority of either process can not be finally ascertained at early stages. Still, early-stage LCA studies can help identify ecological hotspots and guide process development. In particular, the electrochemical CO_2 reduction system results from economic optimization and has not been optimized environmentally. Thus, future works should implement a second environmental target function for the electrolyzer system optimization.

© 2023 The Authors. Advanced Sustainable Systems published by Wiley-VCH GmbH

For the environmental impacts other than GWI, electrochemical CO_2 reduction impacts are higher than SMR impacts in the status quo scenario in 14 out of the 15 categories, as indicated in Figure S19. Most impact categories show decreasing trends along the decarbonization scenarios similar to the GWI. In 11 of 15 categories, however, SMR outperforms electrochemical CO_2 reduction still in the 2050 scenario, indicating a trade-off between impact categories. Since LCA results are generally biased in favor of optimized existing technologies,[83] in-depth studies on burden-shifting are required before implementing electrochemical CO_2 reduction.

3. Conclusions

A process model was developed to optimize the electrochemical production of CO and syngas, including downstream processing of the respective product gases by membrane gas permeation. Our study compares the three ion exchange membranes used in low-temperature CO_2 electrolysis: anion exchange membrane, bipolar exchange membrane, and cation exchange membrane. Besides the economics of the process, we also elucidate the ecological impact of the optimized process by applying LCA.

Our results indicate that the AEM-based electrolyzer is best suited for CO production due to low electricity costs and capital costs for the electrolyzer. The calculated CO production costs of around 796 €/t_{CO} are already competitive to reported market prices for CO. Furthermore, the LCA of the optimized process shows potential for GWI mitigation by electrochemical CO_2 reduction, albeit only if renewable electricity is available. The economic and environmental analyses emphasize that decreasing the electricity consumption of the AEM electrolyzer should be prioritized. Moreover, to replace fossil-based synthesis routes, that is, steam methane reforming completely, not only CO but also H_2 needs to be replaced, calling for continuous improvement of water electrolysis as a key technology for CCU development.

Most surprisingly and against the often ascribed detriment, our study showed that the CO_2 pumping effect in the AEM electrolyzer does not significantly impair the economics of the process. Quite the contrary, the release of CO_2 at the anode and the subsequent separation and recycling using gas permeation offers an efficient indirect regeneration of HCO_3^- and CO_3^{2-}. Future work, therefore, needs to focus on elucidating the energetics and long-term stability of this operation mode.

The BPM electrolyzer configuration shows the lowest production costs for syngas with H_2:CO ratios of 1:1 and 2:1, mainly attributed to the lower costs for additional H_2 production from water electrolysis. The holistic optimization reveals that the process for syngas production is economically more promising when H_2 is purchased from water electrolysis and not co-produced with CO in the CO_2 electrolyzer. Thus, electrochemical membrane reactors for CO_2 reduction to CO need to be optimized for the selective synthesis of CO and not for the co-electrolysis to syngas. This finding is also supported by the strong sensitivity of production costs to changes in Faradaic efficiency, as demonstrated in our sensitivity study.

Moreover, our results highlight membrane-based gas separation as a suitable technology for downstream processing in electrochemical CO_2-to-CO conversion. The low costs of polymeric membrane modules, the variety of selective membrane materials, and the flexibility in flowsheet design offer advantages compared to other conventional separation technologies. Even though product purification contributes slightly to the overall process economics, the LCA showed that recycling of CO_2 should be further optimized to decrease direct emissions and required CO_2 capture. However, we expect a trade-off with the energy consumption of purifying and recycling the off-gas. Hence, bi-objective optimization will be necessary to evaluate this trade-off.

4. Experimental Section

Lead Contact: Further information and requests for resources and materials should be directed to and would be fulfilled by the lead contact, Matthias Wessling (manuscripts.CVT@avt.rwth-aachen.de).

Materials Availability: This study did not generate new unique reagents.

Data and Code Availability: The data and codes used in this study are available from the corresponding authors upon reasonable request.

Overall Process Scheme: Figure 3 shows the block flow diagram of the overall process for electrochemical conversion of CO_2 and H_2O to either pure CO or a mixture of CO and H_2. In the anodic half-cell of the reactor, oxygen evolved from water oxidation in the oxygen evolution reaction. The produced oxygen was vented to the atmosphere in processes with a CEM and BPM electrolyzer. In the case of an AEM electrolyzer, the outlet stream on the anode side also contained CO_2 attributed to carbonate and bicarbonate crossover. In this study, the treatment of the anodic outlet stream was optimized by either venting the CO_2/O_2 mixture or separating and recycling CO_2.

In the cathodic half-cell of the electrolyzer, CO_2 was electrochemically reduced to CO and H_2 evolved in the hydrogen evolution reaction. Both gases left the electrolyzer together with unreacted CO_2 and water vapor resulting from humidification of the CO_2 feed and water uptake in the gas diffusion electrode.

After electrolysis, the resulting gas mixtures were separated to meet the required product specifications. The first step of the downstream processing comprised water removal from the anodic and cathodic outlet gas stream using adsorptive dehumidification. The removal of water was considered to protect the following process units from corrosion, water condensation, or swelling. The anodic and cathodic product streams were separated using membrane gas permeation. The membrane process comprised multi-stage compressors with intercooling and gas permeation membranes. The arrangement of compressors and membranes, the choice of membrane materials, and the recycling of separated CO_2 were degrees of freedom in the optimization. For the production of syngas, water electrolysis was considered to produce pure H_2, which was then mixed with the CO/H_2-rich stream from CO_2 electrolysis. The mixing ratio was optimized by the solver. The process units were explained in more detail in the following sections.

The process model, including models of the different unit operations, was implemented in the General Algebraic Modeling System (GAMS). To optimize the present nonlinear problem (NLP), the Branch-And-Reduce Optimization Navigator (BARON) solver was chosen to find initial values, and the CONOPT solver was applied to identify the optimum. The model structure was adapted from the work of Scholz et al.[84]

Electrolysis Process: For the techno-economic assessment of the electrolysis process, five parameters were required to estimate the economics of the process: 1) the current density (j); 2) the cell voltage (V); 3) the Faradaic efficiency (FE_i) for $i = CO, H_2$; 4) the CO_2 conversion rate; and 5) the geometrical electrode surface area (A_{geom}). This data was usually determined in experiments or calculated using rigorous mathematical models that account for mass transport and electrochemical reaction kinetics. The parameters describing the electrolysis performance in this study were taken from representative experimental studies.[5,11,12] The current density was chosen as the optimization variable. The cell voltage and the Faradaic efficiencies were calculated for the given current density based on

© 2023 The Authors. Advanced Sustainable Systems published by Wiley-VCH GmbH

regression curves that were fitted to experimental data so that each performance indicator is described by

$$y = f(x, \beta),\ y^T = (V, FE_i) \text{ and } x^T = (j) \tag{4}$$

where y is the performance indicator which is either the cell voltage or the Faradaic efficiency, x is the current density that is to be optimized, and β are the fitting parameters β_0, β_1, ..., β_n that are adapted so that the regression curve matches the experimental data. The regression analysis was conducted in Microsoft Excel. The experimental data taken from the literature, the regression curves, and the coefficients of determination were listed in Equations (S1)–(S6), Supporting Information.

The amount of gas produced, $\dot{N}_i$, in the electrochemical reactions is calculated from Faraday's law

$$\dot{N}_i = \frac{j \times FE_i \times A_{\text{geom}}}{z \times F} \tag{5}$$

Here, z is the number of electrons transferred in the electrochemical reaction, and F is the Faraday constant. The conversion rate of CO_2 in the electrolysis was assumed to be constant but was varied within a sensitivity study. The energy consumption of the electrolyzer was calculated from the current density and the cell voltage.

$$P_{\text{elec}} = j \times A_{\text{geom}} \times V \tag{6}$$

Adsorptive Dehumidification: Adsorptive drying of the electrolysis off-gases was considered to minimize the risk of water condensation in the compressors and swelling of the gas separation membrane. The investment and operation costs were approximated using a shortcut equation derived from data from Scholz et al.[85]

Compressor: The compressors were modeled as multi-stage isentropic compression with interstage cooling. The compression ratio and the number of compression stages were optimization variables in this work. The isentropic outlet temperature T_{out} of each compression stage is calculated from

$$T_{\text{out}} = T_{\text{in}} \times \left(\frac{p_{\text{out}}}{p_{\text{in}}}\right)^{(\kappa-1)/\kappa} \tag{7}$$

where T_{in} is the inlet temperature, p_{in} and p_{out} are the inlet and outlet pressure, and κ is the isentropic exponent. The power consumption of the compressors P_c to compress a molar flow $\dot{N}$ is determined by

$$P_c = \dot{N} \times \frac{\kappa}{\kappa - 1} \times R \times (T_{\text{out}} - T_{\text{in}}) \tag{8}$$

Gas Permeation Membrane: Membrane processes were known to be flexible in operation, for example, for fast start-up/shutdown, easily scalable by numbering up, and cost-effective when using polymeric membranes.[48] Furthermore, gas permeation technology was already implemented on a larger scale in, for example, air separation, natural gas processing, and biogas upgrading.[86,87] In this study, different membrane materials for the separation of the electrolysis off-gases had been evaluated.[88–91] The membrane materials had been selected according to reasonable selectivity values and the availability of permeance data for the respective gases. Even though some of these membranes were not yet commercially available, they were based on polymers that were produced on an industrial scale.

The membrane model was discretized along the length using a constant step size. The species flux J_i through the membrane was modeled using the solution-diffusion model (SDM)

$$J_i = Q_i \times \delta \times (y_{r,i} \times p_r - y_{p,i} \times p_p) \tag{9}$$

where Q_i is the permeance of species i in the membrane, δ is the thickness of the selective layer of the membrane, which is assumed to be 0.5 µm for all membrane materials due to missing information in the respective references. $y_{r,i}$ and $y_{p,i}$ are the molar fractions of i in the retentate and the permeate, respectively. p_r and p_p are the absolute pressures on the feed and permeate side.

Temperature gradients due to heat dissipation, the Joule–Thomson effect, and pressure losses were neglected. Furthermore, constant permeances and ideal gas behavior were assumed. The membrane module configuration, the membrane material selection, the membrane area, and the stage-cut were optimized in this study. Figure S4, Supporting Information, presents the considered process configurations.

The gas permeation process for separating the anodic outlet gas stream was modeled using a surrogate model in the overall process flowsheet to reduce complexity and computational costs. The surrogate model was derived from separate simulations in which the aforementioned membrane processes were optimized for different CO_2:O_2 ratios and flow rates. The optimization results were fed into a regression model to fit the anodic gas separation performance.

Economic Evaluation: For the optimization of the process, the specific production costs PC (€/t_{product}) of either CO or syngas were chosen as the objective function. Thus, the optimization problem was to minimize PC.

$$PC = \frac{1}{m_{\text{product}}} \times (CC_{\text{total}} \times d_{\text{year}} + OC_{\text{total}}) \tag{10}$$

Here, m_{product} is the mass of product per year, CC_{total} are the capital costs of the plant, d_{year} is the depreciation factor calculated from the lifetime of the plant and the interest rate, and OC_{total} are the yearly operational costs. The production capacity of the plant is set to 80 000 t_{CO} a^{-1}, which is the amount required for producing, for example, toluene diisocyanates (TDIs) in a typical world-scale plant, assuming stoichiometric conversion.[92] For comparison of the CO and the syngas production processes, the higher heating value HHV_i of the final product stream was taken constant. The heating value defined the amount of energy in the fuel (here, either CO or syngas). The heating value for a product stream of 80 000 t_{CO} a^{-1} calculated to 808 900 MJ a^{-1}. From this value, the amount of syngas to be produced was calculated as 45 200 t a^{-1} (1:1) and 32 900 t a^{-1} (2:1). The HHV_i for CO and H_2 is tabulated in Table S2, Supporting Information.

Capital Costs: The capital costs are the sum of the capital costs of each process unit. The capital costs of the electrolyzer $CC_{\text{electrolyzer}}$ were calculated based on an investment cost analysis for a H_2 fuel cell.[93] The bare module costs $BC_{\text{electrolyzer}}$ of the electrolyzer were calculated per geometric electrode area and comprised cost for the electrodes, the ion exchange membrane, and surroundings, including aluminum end plates, bipolar graphite plates, and busbars for electricity supply. All parameters on the calculation of the $BC_{\text{electrolyzer}}$ for each electrolyzer type are given in the Supporting Information.

$$CC_{\text{electrolyzer}} = BC_{\text{electrolyzer}} \times A_{\text{geom}} \tag{11}$$

Capital costs for the compressor $CC_{\text{compressor}}$ were estimated with Guthrie's method.[94,95] This method allowed the calculation of the bare module costs of the compressor $BC_{\text{compressor}}$ based on reference costs C_0 for the equipment with a reference compression duty S_0.

$$BC_{\text{compressor}} = C_0 \times \left(\frac{S}{S_0}\right)^{\alpha} \tag{12}$$

In this equation, S is the required compression duty determined in the optimization, and α is the scaling factor, which considered the economy of scale and is, therefore, lower than 1. The reference values and the scaling factor were taken from Biegler at al.[94] and are tabulated in Table S1, Supporting Information. The capital costs of the compressor were then calculated to

$$CC_{\text{compressor}} = BC_{\text{compressor}} \times UF \times (MPF + MF - 1) \tag{13}$$

© 2023 The Authors. Advanced Sustainable Systems published by Wiley-VCH GmbH

where UF is the update factor, MPF is the material and pressure factor, and MF is the module factor. UF took into account the change in price level between 1969 and now. MPF and MF accounted for the material and size of the compressor.

The capital costs of the membrane module $CC_{membrane}$ were calculated based on the required membrane surface area A_{mem} and area-specific membrane module costs for polymeric membranes $BC_{membrane}$, listed in Table S1, Supporting Information.[96]

$$CC_{membrane} = BC_{membrane} \times A_{mem} \tag{14}$$

Capital costs for drying the electrolysis off-gas before compression were calculated using data for adsorptive drying from Scholz et al.[85]

Operation Costs: Operation costs included expenditure on utilities $OC_{utilities}$, that is, energy and reactants, CO_2 emissions $OC_{emissions}$, replacement of electrolyzer, and gas permeation membrane components $OC_{replacement}$, as well as maintenance costs $OC_{maintenance}$.

$$OC_{total} = OC_{utilities} + OC_{emissions} + OC_{replacement} + OC_{maintenance} \tag{15}$$

Energy was consumed in the electrolyzer and the compressor units. The utility costs for electrical energy $UC_{electricity}$ in the base case scenario are taken to 0.09 €/kWh. The utility costs for reactants UC_i comprise CO_2 and H_2 from water electrolysis. Expenses for water were neglected. For the base case, a CO_2 price of 25 $/t was assumed, which was calculated for carbon capture from flue gas.[97] For the AEM electrolyzer, the ratio of recycling CO_2 from the anodic off-gas is a degree of freedom in the optimization. In the case of recycling, the expenses for purifying CO_2 from the anode were considered according to Equation (S9), Supporting Information. Costs for H_2 were considered for the production of syngas. H_2 was produced in water electrolysis and implemented as a shortcut equation described in theSupporting Information. The ratio of purchased H_2 from water electrolysis is optimized in this study. The operation costs for utilities are calculated to

$$OC_{utilities} = t_{year} \times \left(UC_{electricity} \times (P_c + P_{elec}) + UC_{CO_2} \times \dot{m}_{feed,CO_2} + UC_{H_2} \times \dot{m}_{water\ electrolysis,H_2} \right) \tag{16}$$

In this equation, t_{year} is the annual operation time of the plant, and $\dot{m}_{feed,CO_2}$ and $\dot{m}_{water\ electrolysis,H_2}$ are the required mass streams of CO_2 in the feed of the CO_2 electrolyzer and H_2 from water electrolysis, both calculated in the optimization.

As CO_2 was separated from the desired product but not fully recycled, additional costs for the emission of purged CO_2, $\dot{m}_{purge,CO_2}$, need to be considered. Emission costs were also considered for the processes with an AEM electrolyzer, where CO_2 is not recovered from the anodic off-gas. Emitters of CO_2 need to buy certificates from the European Union to release CO_2 to the environment. The CO_2 certificate price EC_{CO2} assumed in this study is 25 €/t.

$$OC_{emissions} = EC_{CO2} \times \dot{m}_{purge,CO_2} \times t_{year} \tag{17}$$

Replacement of the electrodes, the ion exchange membrane, and the gas permeation membrane was also considered in the operation costs. The lifetime, $t_{lifetime}$, of the electrodes and ion exchange membrane was taken to 2.5 years.[98] After this operation period, the parts had to be exchanged. For the gas permeation membranes, a lifetime of 5 years was assumed.[96] The replacement costs were summed up over the plant lifetime, t_{plant}, of 20 years and then depreciated per year.

$$OC_{replacement} = d_{year} \times t_{plant} \times \left(\frac{1}{t_{lifetime,\ electrolyzer}} \times (BC_{IEM} + BC_{catalyst}) + \frac{1}{t_{lifetime,\ membrane}} \times BC_{membrane} \right) \tag{18}$$

Maintenance of the components of the CO_2 electrolyzer and the gas permeation membrane process was assumed to be 2.5% of the total capital costs depreciated per year.

Life-Cycle Assessment: While the motivation for developing carbon capture and utilization (CCU) processes was greenhouse gas (GHG) emission mitigation, this goal was not always achieved. For instance, GHG emissions from fossil-based energy consumed by the CO_2-based route could outweigh the GHG reduction from CO_2 capture. In order to ensure targeted global warming impact (GWI) mitigation compared to the incumbent technology, a thorough environmental assessment of the electrochemical CO_2 reduction process was necessary. LCA is a holistic method to assess the environmental impact of products and services across the entire life cycle, that is, "from cradle to grave". The LCA methodology is standardized in ISO 14040 and ISO 14044.[56,57]

LCA studies of CO_2-based CO production in the literature cover multiple routes: reverse water-gas-shift (rWGS),[80,81,99–101] dry reforming of methane (DRM),[80,81,99,100] A solid oxide electrolyzer cell (SOEC) route,[101] and the purification of CO-containing basic oxygen furnace gas[102] had been assessed in comparison to the fossil benchmark technology, namely, steam methane reforming (SMR). The studies concluded that rWGS and DRM supplied with current electricity mixes were not competitive to SMR in terms of GWI.[80,81,99,100] However, the GWI of rWGS and DRM decreased with increasing shares of renewable electricity generation, allowing GWI mitigation compared to SMR.[100] Main contributors to the GWI were H_2 production and the electricity demand.[80,81,99–101]

Kibria Nabil et al.[101] approximate the SOEC for CO production with an energy demand from industrially available CO_2 electrolyzers. The authors found the SOEC route to perform better in terms of GWI than both rWGS and SMR at a 50% share of renewable electricity and recommend renewable syngas production as a promising case for industrial application. Some general insights result from the limited number[103] of LCA studies on products of electrochemical CO_2 reduction: Electricity requirements for conversion and product separation were the biggest contributors to GWI for gas and liquid products, respectively.[101] Accordingly, the electricity supply's GWI was a main influencing parameter in LCA of electrochemical CO_2 reduction.[101,103] At the methodological level, Somoza–Tornos et al.[103] found that LCA studies on electrochemical CO_2 reduction use differing assumptions, particularly concerning multifunctionality, that is, the co-production of multiple valuable products. Specifically, the avoidance of conventional co-product production may result in a carbon credit or "avoided burden" for the studied process.[56,57] For instance, Kibria Nabil et al.[101] assumed a carbon credit for H_2 as a byproduct of electrochemical CO_2 reduction processes. The authors noted that H_2, although co-produced only in small amounts, impacts the GWI significantly due to the high emission intensity of conventional H_2 production.

In comparative LCA studies, the LCA practitioner might exclude identical life-cycle stages for all compared systems.[56,57] For instance, fossil and CO_2-based production processes yielding an identical product (either CO or syngas), rendering the use phase and disposal of the product identical between production processes were compared. Thus, a "cradle to gate" LCA study in this work, which includes the extraction of resources and the supply chain up to the production of the studied product was performed.

According to ISO 14040,[56] production systems could only be compared fairly if they fulfill the same function. Thus, the so-called "functional unit" is defined, which quantitatively described the qualitative function of a system and served as a basis for comparison. The function of the electrochemical CO_2 reduction process is the production of a given amount of either pure CO or syngas with an H_2:CO molar ratio of either 2:1 or 1:1. In contrast, the conventional steam methane reforming (SMR) process produced syngas with a 3:1 molar ratio,[80] rendering a direct comparison unfair. To enable the comparison of SMR and electrochemical CO_2 reduction, system expansion was applied and the functional unit was defined as the production of 1 kg CO and 0.216 kg H_2, which corresponded to a 3:1 molar ratio as illustrated in **Figure 13**.

Electrochemical CO_2 reduction was modeled according to the process configuration identified as most promising from the economic optimization and is introduced in the results section. Since electrochemical CO_2 reduction produced either pure CO or synthesis gas with a H_2:CO ratio

© 2023 The Authors. Advanced Sustainable Systems published by Wiley-VCH GmbH

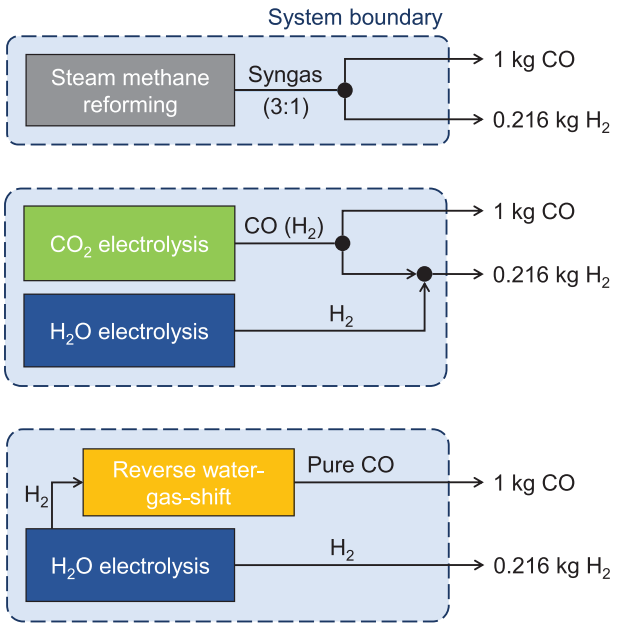

Figure 13. System boundaries and functional unit of the LCA study.

lower than 3:1, the remaining part of H_2 required for the functional unit was assumed to be produced by alkaline water electrolysis. CO production by reverse Water-Gas-Shift (rWGS) is modeled according to Sternberg et al.[80] To produce the functional unit, the rWGS system was equally expanded by H_2 production from alkaline electrolysis.

Since the literature showed that the environmental impact of CCU technologies varies drastically with the assumptions made for electricity, heat, and CO_2 feedstock supply,[104,105] a sensitivity analysis on these assumptions was provided. Particularly, the environmental impact in four scenarios representing different decarbonization levels was evaluated as introduced in Table 5. As background data for the LCA study, the ecoinvent v3.8 database was used in the cutoff system model where not otherwise specified.[106] The system model specified how end-of-life recycling emissions were handled in the calculations. The ecoinvent association recommended using the cutoff system model.[107]

An electricity grid mix was calculated for each scenario, which was supplied to electrochemical CO_2 reduction, rWGS, and water electrolysis. To be consistent with the electricity prices assumed in the economic optimization, the German electricity mixes were modeled for 2030 and 2050 according to prognoses by the Institute of energy economics at the University of Cologne (EWI).[68] For detailed information on electricity modeling for the scenarios EWI 2030 and EWI 2050, please refer to the Supporting Information. For the status quo scenario, the current German electricity mix[106] was chosen, which is the basis of the EWI scenarios. Finally, a scenario with 100% wind electricity was considered a lower boundary for the GWI of electricity production.

Heat production was assumed from electricity with a conservative 95% efficiency for all scenarios except the status quo, where heat was produced via the combustion of fossil fuels. As the CO_2 source, carbon capture from a coal-fired power plant was assumed for the status quo and EWI 2030 scenarios, modeled according to Schreiber et al.[108] With higher levels of renewable electricity production, carbon capture from a coal-fired power plant cannot be assumed as the standard technology. Instead, direct air capture (DAC)[104] was considered for the EWI 2050 and wind power only scenarios. H_2 was assumed to be produced from alkaline water electrolysis in all scenarios and modeled according to Koj et al.[109]

Both electrochemical CO_2 reduction and rWGS produced some off-heat, which cannot be used directly in the respective processes. Since heat integration with other processes was not necessarily possible, any off-heat was assumed to be dissipated. For the impact assessment, the Environmental Footprint 3.0 methodology is employed, as recommended by the European Commission.[58]

Supporting Information

Supporting Information is available from the Wiley Online Library or from the author.

Acknowledgements

This research did not receive any specific grant from funding agencies in the public, commercial, or not-for-profit sectors. M.W. acknowledges DFG funding through the Gottfried Wilhelm Leibniz Prize 2019.

Open access funding enabled and organized by Projekt DEAL.

Conflict of Interest

The authors declare no conflict of interest.

Author Contributions

M.H.: conceptualization, methodology, software, validation, investigation, data curation, writing—original draft, writing—review and editing, visualization; H.M.: conceptualization, methodology, investigation, data curation, writing—original draft, writing—review and editing. T.G.: conceptualization, methodology, software, validation, investigation, data curation, writing—review and editing. R.G.K.: conceptualization, writing—review and editing, supervision, project administration. A.B.: conceptualization, writing—review and editing, supervision. M.W.: conceptualization, writing—review and editing, supervision, funding acquisition, project administration.

Data Availability Statement

The data that support the findings of this study are available from the corresponding author upon reasonable request.

Keywords

carbon utilization, electrochemical CO_2 reduction, holistic process optimization, life-cycle assessment, techno-economic assessment

Received: February 21, 2023
Revised: March 29, 2023
Published online: May 14, 2023

[1] A. Kätelhön, R. Meys, S. Deutz, S. Suh, A. Bardow, *Proc. Natl. Acad. Sci. USA* **2019**, *116*, 11187.
[2] J. L. Barton, *Science* **2020**, *368*, 1181.
[3] Z. J. Schiffer, K. Manthiram, *Joule* **2017**, *1*, 10.
[4] S. Hernández, M. A. Farkhondehfal, F. Sastre, M. Makkee, G. Saracco, N. Russo, *Green Chem.* **2017**, *19*, 2326.
[5] Z. Liu, H. Yang, R. Kutz, R. I. Masel, *J. Electrochem. Soc.* **2018**, *165*, J3371.
[6] T. Haas, R. Krause, R. Weber, M. Demler, G. Schmid, *Nat. Catal.* **2018**, *1*, 32.

© 2023 The Authors. Advanced Sustainable Systems published by Wiley-VCH GmbH

[7] G. O. Larrazábal, P. Strøm-Hansen, J. P. Heli, K. Zeiter, K. T. Therkildsen, I. Chorkendorff, B. Seger, *ACS Appl. Mater. Interfaces* **2019**, *11*, 41281.
[8] F. P. G. De Arquer, C.-T. Dinh, A. Ozden, J. Wicks, C. McCallum, A. R. Kirmani, D.-H. Nam, C. Gabardo, A. Seifitokaldani, X. Wang, Y. C. Li, F. Li, J. Edwards, L. J. Richter, S. J. Thorpe, D. Sinton, E. H. Sargent, *Science* **2020**, *367*, 661.
[9] S. S. Bhargava, F. Proietto, D. Azmoodeh, E. R. Cofell, D. A. Henckel, S. Verma, C. J. Brooks, A. A. Gewirth, P. J. Kenis, *ChemElectroChem* **2020**, *7*, 2001.
[10] U. O. Nwabara, A. D. Hernandez, D. A. Henckel, X. Chen, E. R. Cofell, M. P. De-Heer, S. Verma, A. A. Gewirth, P. J. Kenis, *ACS Appl. Energy Mater.* **2021**, *4*, 5175.
[11] D. A. Salvatore, D. M. Weekes, J. He, K. E. Dettelbach, Y. C. Li, T. E. Mallouk, C. P. Berlinguette, *ACS Energy Lett.* **2017**, *3*, 149.
[12] J.-B. Vennekoetter, R. Sengpiel, M. Wessling, *Chem. Eng. J.* **2019**, *364*, 89.
[13] L. Ma, S. Fan, D. Zhen, X. Wu, S. Liu, J. Lin, S. Huang, W. Chen, G. He, *Ind. Eng. Chem. Res.* **2017**, *56*, 10242.
[14] C. M. Gabardo, C. P. O'Brien, J. P. Edwards, C. McCallum, Y. Xu, C.-T. Dinh, J. Li, E. H. Sargent, D. Sinton, *Joule* **2019**, *3*, 2777.
[15] T. Zheng, K. Jiang, N. Ta, Y. Hu, J. Zeng, J. Liu, H. Wang, *Joule* **2019**, *3*, 265.
[16] M. Ma, E. L. Clark, K. T. Therkildsen, S. Dalsgaard, I. Chorkendorff, B. Seger, *Energy Environ. Sci.* **2020**, *13*, 977.
[17] J. A. Rabinowitz, M. W. Kanan, *Nat. Commun.* **2020**, *11*, 5231.
[18] D. A. Salvatore, C. M. Gabardo, A. Reyes, C. P. O'Brien, S. Holdcroft, P. Pintauro, B. Bahar, M. Hickner, C. Bae, D. Sinton, E. H. Sargent, C. P. Berlinguette, *Nat. Energy* **2021**, *6*, 339.
[19] Y. Zhao, H. Yu, D. Yang, J. Li, Z. Shao, B. Yi, *J. Power Sources* **2013**, *221*, 247.
[20] A. D. Mohanty, S. E. Tignor, J. A. Krause, Y.-K. Choe, C. Bae, *Macromolecules* **2016**, *49*, 3361.
[21] B. Endrődi, E. Kecsenovity, A. Samu, T. Halmágyi, S. Rojas-Carbonell, L. Wang, Y. Yan, C. Janáky, *Energy Environ. Sci.* **2020**, *13*, 4098.
[22] Z. Yin, H. Peng, X. Wei, H. Zhou, J. Gong, M. Huai, L. Xiao, G. Wang, J. Lu, L. Zhuang, *Energy Environ. Sci.* **2019**, *12*, 2455.
[23] A. Pătru, T. Binninger, B. Pribyl, T. J. Schmidt, *J. Electrochem. Soc.* **2019**, *166*, F34.
[24] J. Y. Kim, P. Zhu, F.-Y. Chen, Z.-Y. Wu, D. A. Cullen, H. Wang, *Nat. Catal.* **2022**, *5*, 288.
[25] C. P. O'Brien, R. K. Miao, S. Liu, Y. Xu, G. Lee, A. Robb, J. E. Huang, K. Xie, K. Bertens, C. M. Gabardo, J. P. Edwards, C.-T. Dinh, E. H. Sargent, D. Sinton, *ACS Energy Lett.* **2021**, *6*, 2952.
[26] C. Shen, R. Wycisk, P. N. Pintauro, *Energy Environ. Sci.* **2017**, *10*, 1435.
[27] J.-B. Vennekötter, T. Scheuermann, R. Sengpiel, M. Wessling, *J. CO2 Util.* **2019**, *32*, 202.
[28] M. A. Blommaert, S. Subramanian, K. Yang, W. A. Smith, D. A. Vermaas, *ACS Appl. Mater. Interfaces* **2021**, *14*, 557.
[29] L. Chen, Q. Xu, S. Z. Oener, K. Fabrizio, S. W. Boettcher, *Nat. Commun.* **2022**, *13*, 3846.
[30] R. A. Tufa, D. Chanda, M. Ma, D. Aili, T. B. Demissie, J. Vaes, Q. Li, S. Liu, D. Pant, *Appl. Energy* **2020**, *277*, 115557.
[31] H. Li, H. Li, P. Wei, Y. Wang, Y. Zang, D. Gao, G. Wang, X. Bao, *Energy Environ. Sci.* **2023**, *16*, 1502.
[32] Z. Liu, T. Yan, H. Shi, H. Pan, Y. Cheng, P. Kang, *ACS Appl. Mater. Interfaces* **2022**, *14*, 7900.
[33] B. Pan, J. Fan, J. Zhang, Y. Luo, C. Shen, C. Wang, Y. Wang, Y. Li, *ACS Energy Lett.* **2022**, *7*, 4224.
[34] M. Lin, L. Han, M. R. Singh, C. Xiang, *ACS Appl. Energy Mater.* **2019**, *2*, 5843.
[35] D. Salvatore, C. P. Berlinguette, *ACS Energy Lett.* **2019**, *5*, 215.
[36] M. Ma, S. Kim, I. Chorkendorff, B. Seger, *Chem. Sci.* **2020**, *11*, 8854.
[37] K. Xie, R. K. Miao, A. Ozden, S. Liu, Z. Chen, C.-T. Dinh, J. E. Huang, Q. Xu, C. M. Gabardo, G. Lee, J. P. Edwards, C. P. O'Brien, S. W. Boettcher, D. Sinton, E. H. Sargent, *Nat. Commun.* **2022**, *13*, 3609.
[38] B. Eriksson, T. Asset, F. Spanu, F. Lecoeur, M. Dupont, F. Garces-Pineda, J. R. G. Mascaros, S. Cavaliere, J. Rozière, F. Jaouen, *J. Electrochem. Soc.* **2022**, *169*, 034508.
[39] S. Verma, B. Kim, H.-R. Jhong, S. Ma, P. J. Kenis, *ChemSusChem* **2016**, *9*, 1972.
[40] X. Li, P. Anderson, H.-R. M. Jhong, M. Paster, J. F. Stubbins, P. J. Kenis, *Energy Fuels* **2016**, *30*, 5980.
[41] J. M. Spurgeon, B. Kumar, *Energy Environ. Sci.* **2018**, *11*, 1536.
[42] M. Jouny, W. Luc, F. Jiao, *Ind. Eng. Chem. Res.* **2018**, *57*, 2165.
[43] M. Rumayor, A. Dominguez-Ramos, P. Perez, A. Irabien, *J. CO2 Util.* **2019**, *34*, 490.
[44] H. Shin, K. U. Hansen, F. Jiao, *Nat. Sustain.* **2021**, *4*, 911.
[45] T. Alerte, J. P. Edwards, C. M. Gabardo, C. P. O'Brien, A. Gaona, J. Wicks, A. Obradović, A. Sarkar, S. A. Jaffer, H. L. MacLean, D. Sinton, E. H. Sargent, *ACS Energy Lett.* **2021**, *6*, 4405.
[46] B. Pribyl-Kranewitter, A. Beard, C. Gîjiu, D. Dinculescu, T. Schmidt, *Renewable Sustainable Energy Rev.* **2022**, *154*, 111807.
[47] K. Roh, L. Brée, P. Schäfer, D. Strohmeier, A. Mitsos, *IFAC-PapersOnLine* **2021**, *55*, 298.
[48] R. W. Baker, *Membrane Technology and Applications*, 2nd ed., John Wiley & Sons, Hoboken, Germany **2004**.
[49] M. Scholz, T. Melin, M. Wessling, *Renewable Sustainable Energy Rev.* **2013**, *17*, 199.
[50] S. Alsayegh, J. Johnson, X. Wei, B. Ohs, J. Lohaus, M. Wessling, *Int. J. Hydrogen Energy* **2017**, *42*, 21793.
[51] K. Roh, A. Bardow, D. Bongartz, J. Burre, W. Chung, S. Deutz, D. Han, M. Heßelmann, Y. Kohlhaas, A. König, J. S. Lee, R. Meys, S. Völker, M. Wessling, J. H. Lee, A. Mitsos, *Green Chem.* **2020**, *22*, 3842.
[52] S. K. Nabil, S. McCoy, M. G. Kibria, *Green Chem.* **2021**, *23*, 867.
[53] J. Heuser, H. Kauth, C. Kords, US Patent 6,930,202, **2005**.
[54] H. Weber, J. Falbe, *Ind. Eng. Chem.* **1970**, *62*, 33.
[55] Y. Lu, T. Lee, *J. Natural Gas Chem.* **2007**, *16*, 329.
[56] International Organization for Standardization, Environmental management—life cycle assessment—principles and framework, https://www.iso.org/standard/37456.html (accessed: October 2020).
[57] Environmental management — life cycle assessment — requirements and guidelines, https://www.iso.org/standard/38498.html (accessed: October 2020).
[58] S. Fazio, F. Biganzioli, V. De Laurentiis, L. Zampori, S. Sala, E. Diaconu, Supporting information to the characterisation factors of recommended ef life cycle impact assessment methods, version 2, JRC Publications Repository, Publications Office of the European Union, Luxembourg **2018**.
[59] B. Kim, S. Ma, H.-R. M. Jhong, P. J. Kenis, *Electrochim. Acta* **2015**, *166*, 271.
[60] M. Heßelmann, B. C. Bräsel, R. G. Keller, M. Wessling, *Electrochem. Sci. Adv.* **2022**, *3*, 2100160.
[61] R. I. Masel, Z. Liu, H. Yang, J. J. Kaczur, D. Carrillo, S. Ren, D. Salvatore, C. P. Berlinguette, *Nat. Nanotechnol.* **2021**, *16*, 118.
[62] M. C. Monteiro, M. F. Philips, K. J. P. Schouten, M. Koper, *Nat. Commun.* **2021**, *12*, 4943.
[63] J. E. Huang, F. Li, A. Ozden, A. Sedighian Rasouli, F. P. García de Arquer, S. Liu, S. Zhang, M. Luo, X. Wang, Y. Lum, Y. Xu, K. Bertens, R. K. Miao, C.-T. Dinh, D. Sinton, E. H. Sargent, *Science* **2021**, *372*, 1074.
[64] Y. Xie, P. Ou, X. Wang, Z. Xu, Y. C. Li, Z. Wang, J. E. Huang, J. Wicks, C. McCallum, N. Wang, Y. Wang, T. Chen, B. T. W. Lo, D. Sinton, J. C. Yu, Y. Wang, E. H. Sargent, *Nat. Catal.* **2022**, *5*, 564.

© 2023 The Authors. Advanced Sustainable Systems published by Wiley-VCH GmbH

[65] Y. Hua, J. Wang, T. Min, Z. Gao, *J. Power Sources* **2022**, *535*, 231453.
[66] Á. Vass, A. Kormányos, Z. Kószó, B. Endrodi, C. Janáky, *ACS Catal.* **2022**, *12*, 1037.
[67] A. Breitkopf, Strompreise für industriekunden in ländern europas 2018, https://de.statista.com/ (accessed: October 2020).
[68] M. Gierkink, D. Lencz, F. Arnold, Auswirkungen einer beendigung der kohleverstromung bis 2038 auf den strommarkt, CO^2-emissionen und ausgewählte industrien: Eine analyse des abschlussberichts der wsb-kommission.
[69] IEA, Norway - Energy System Overview, https://www.iea.org/countries/norway (accessed: May 2022).
[70] W. Li, Z. Yin, Z. Gao, G. Wang, Z. Li, F. Wei, X. Wei, H. Peng, X. Hu, L. Xiao, J. Lu, L. Zhuang, *Nat. Energy* **2022**, *7*, 835.
[71] Y. Xu, J. P. Edwards, S. Liu, R. K. Miao, J. E. Huang, C. M. Gabardo, C. P. O'Brien, J. Li, E. H. Sargent, D. Sinton, *ACS Energy Lett.* **2021**, *6*, 809.
[72] K. V. Petrov, J. Bui, L. M. Baumgartner, L.-C. Weng, S. Dischinger, D. M. Larson, D. Miller, A. Z. Weber, D. A. Vermaas, *Sustainable Energy Fuels* **2022**, *6*, 5077.
[73] P. Jeanty, C. Scherer, E. Magori, K. Wiesner-Fleischer, O. Hinrichsen, M. Fleischer, *J. CO2 Util.* **2018**, *24*, 454.
[74] E. Jeng, F. Jiao, *React. Chem. Eng.* **2020**, *5*, 1768.
[75] D. W. Keith, G. Holmes, D. S. Angelo, K. Heidel, *Joule* **2018**, *2*, 1573.
[76] J. Parrondo, C. G. Arges, M. Niedzwiecki, E. B. Anderson, K. E. Ayers, V. Ramani, *Rsc Adv.* **2014**, *4*, 9875.
[77] G. T. Rochelle, *Science* **2009**, *325*, 1652.
[78] H. Lepaumier, E. F. da Silva, A. Einbu, A. Grimstvedt, J. N. Knudsen, K. Zahlsen, H. F. Svendsen, *Energy Proc.* **2011**, *4*, 1652.
[79] K. Xie, A. Ozden, R. K. Miao, Y. Li, D. Sinton, E. H. Sargent, *Nat. Commun.* **2022**, *13*, 3070.
[80] A. Sternberg, C. M. Jens, A. Bardow, *Green Chem.* **2017**, *19*, 2244.
[81] T. Langhorst, S. McCord, A. Zimmermann, L. Müller, L. Cremonese, T. Strunge, Y. Wang, A. V. Zaragoza, J. Wunderlich, A. Marxen, K. Armstrong, G. Buchner, A. Kätelhön, M. Bachmann, A. Sternberg, S. Michailos, H. Naims, B. Winter, D. Roskosch, G. Faber, C. Mangin, B. Olfe-Kräutlein, P. Styring, R. Schomäcker, A. Bardow, V. Sick, Techno-economic assessment and life cycle assessment guidelines for CO_2 utilization (version 2.0), Technical Report, Global CO_2 Initiative, University of Michigan, Michigan **2022**. https://doi.org/10.7302/4190.
[82] F. Piccinno, R. Hischier, S. Seeger, C. Som, *J. Cleaner Prod.* **2016**, *135*, 1085.
[83] P. Jessop, *Green Chem.* **2020**, *22*, 13.
[84] M. Scholz, M. Alders, T. Lohaus, M. Wessling, *J. Membr. Sci.* **2015**, *474*, 1.
[85] M. Scholz, B. Frank, F. Stockmeier, S. Falß, M. Wessling, *Ind. Eng. Chem. Res.* **2013**, *52*, 16929.
[86] R. W. Baker, *Ind. Eng. Chem. Res.* **2002**, *41*, 1393.
[87] X. Y. Chen, H. Vinh-Thang, A. A. Ramirez, D. Rodrigue, S. Kaliaguine, *RSC Adv.* **2015**, *5*, 24399.
[88] Y. Alqaheem, A. Alomair, M. Vinoba, A. Perez, *Int. J. Polym. Sci.* **2017**, *2017*, 4250927.
[89] R. S. Murali, S. Sridhar, T. Sankarshana, Y. Ravikumar, *Ind. Eng. Chem. Res.* **2010**, *49*, 6530.
[90] O. C. David, D. Gorri, A. Urtiaga, I. Ortiz, *J. Membr. Sci.* **2011**, *378*, 359.
[91] C. Aitken, W. Koros, D. Paul, *Macromolecules* **1992**, *25*, 3424.
[92] Covestro AG, Gas Phase Technology: 60% Less Energy Consumption, https://www.covestro.com/ (accessed: April 2021).
[93] Manufacturing cost analysis of 10 kw and 25 kw direct hydrogen polymer electrolyte membrane (pem) fuel cell for material handling applications, Technical Report, Battelle Memorial Institute, Columbus **2013**.
[94] L. T. Biegler, I. E. Grossmann, A. W. Westerberg, *Systematic Methods of Chemical Process Design*, Prentice-Hall International Series in the Physical and Chemical Engineering Sciences, Prentice-Hall, Upper Saddle River, NJ **1997**.
[95] H. Guthrie, *Chem. Eng* **1969**, *32*, 114.
[96] L. Zhao, R. Menzer, E. Riensche, L. Blum, D. Stolten, *Energy Proc.* **2009**, *1*, 269.
[97] M. Schneider, M. Romer, M. Tschudin, H. Bolio, *Cem. Concr. Res.* **2011**, *41*, 642.
[98] J. T. Smolinka, M. Günther, Studie: Stand und Entwicklungspotenzial der Wasserelektrolyse zur Herstellung von Wasserstoff aus regenerativen Energien, https://www.now-gmbh.de/projektfinder/studie-wasserelektrolyse/ (accessed: October 2020).
[99] N. Thonemann, M. Pizzol, *Energy Environ. Sci.* **2019**, *12*, 2253.
[100] N. Thonemann, *Appl. Energy* **2020**, *263*, 114599.
[101] S. Kibria Nabil, S. McCoy, M. G. Kibria, *Green Chem.* **2021**, *23*, 867.
[102] J. Hense, M. Bachmann, L. Polte, N. von der Aßen, A. Jupke, *Chem. Ing. Tech.* **2022**, *94*, 1524.
[103] A. Somoza-Tornos, O. J. Guerra, A. M. Crow, W. A. Smith, B.-M. Hodge, *iScience* **2021**, *24*, 102813.
[104] N. von der Assen, J. Jung, A. Bardow, *Energy Environ. Sci.* **2013**, *6*, 2721.
[105] A. W. Zimmermann, L. Müller, Y. Wang, Techno-economic assessment & life cycle assessment guidelines for CO_2 utilization (version 1.1), Global CO_2 Initiative, University of Michigan, Michigan **2020**.
[106] G. Wernet, C. Bauer, B. Steubing, J. Reinhard, E. Moreno-Ruiz, B. Weidema, *Int. J. Life Cycle Assess.* **2016**, *21*, 1218.
[107] ecoinvent Association, System models, https://ecoinvent.org/the-ecoinvent-database/system-models/, **2022**, Accessed: 2022-03-24.
[108] A. Schreiber, P. Zapp, W. Kuckshinrichs, *Int. J. Life Cycle Assess.* **2009**, *14*, 547.
[109] J. C. Koj, C. Wulf, A. Schreiber, P. Zapp, *Energies* **2017**, *10*, 860.

© 2023 The Authors. Advanced Sustainable Systems published by Wiley-VCH GmbH